UNIVERSIDADE D
COIMBRA

Rita Pereira Ângelo

THE ROLE OF PROSTATE DUCTS IN PROSTATE CANCER PROGRESSION

A COMPUTATIONAL MODEL

Dissertação no âmbito do Mestrado em Biologia Computacional orientada pelos Professores Doutores Rui Davide Martins Travasso e Guillermo Lorenzo Gómez e apresentada ao Departamento de Ciências da Vida da Faculdade de Ciências e Tecnologia da Universidade de Coimbra.

Julho de 2023

1 2  9 0

UNIVERSIDADE D
COIMBRA

Master's in Computational Biology

The Role of Prostate Ducts in Prostate Cancer Progression

Rita Pereira Ângelo

Supervisor:

Ph.D. Rui Travasso

Co-Supervisor:

Ph.D. Guillermo Lorenzo

Thesis submitted to the Faculty of Sciences and Technology of the University of Coimbra in fulfillment of the requirements for the Master's Degree in Computational Biology.

Coimbra, July 2023

Project developed in collaboration with:

Contributions and Funding. I, Rita Pereira Ângelo, declare to have fully written and perform the research behind this thesis. In addition, I declare that this thesis has not been previously submitted, as a whole or in part, to obtain another graduation level. This work was funded by FEDER funds through the Operational Programme Competitiveness Factors - COMPETE and by national funds by FCT - Foundation for Science and Technology under the projects UIDB/04564/2020 and UIDP/04564/2020.

Acknowledgments

I have learned so much. Not only during the making of this thesis but in the past two years. This would not have been possible without all the Professors that introduced Computational Biology to me. Thank you all for your hard work.

Most specially, Professor Rui Travasso deserves my gratitude for welcoming me into this new-found world of biological modelling, for guiding me in this process and for his positivism, patience and advice. A warm thank you is due to Professor Guillermo Lorenzo, for his incredible insight, suggestions and corrections.

I also want to acknowledge everyone at CFisUC for being kind to me, for the laughs we had (almost) every Friday, and for all the interesting discussions about everyone's work.

My gratitude goes also to Alexandra Elbakyan. I cannot imagine how much poorer this work would have been if not for Alexandra's fight for open and accessible science.

The friends I gained in this new city of Coimbra also deserve my acknowledgment. Thank you Inês for being my sister in the midst of chaos, for every night we spent laughing so we wouldn't cry. Thank you Maria João for all the support, for all the afternoons of coffee dates and for our study nights. I am so grateful for having met José, Elmer, Ana Beatriz, and Ricardo, my colleagues and friends who were always ready to give encouraging words and all the help they could. I will never forget all the good times we had in the last couple of years.

To my favourite biochemist, Ana "Peixinho" Paula, who despite being far away never failed to check up on me, you will never know how much you helped me and how grateful I am.

Alex, thank you for making me laugh when I was too serious, for the silly and lovely letters we exchanged, for your immediate and unreserved support since the beginning and for going the distance (literally). Infinity thousand plus one, always.

Finally, thank you isn't enough to my mother, Telma, without whom I would not have the opportunity to keep studying. I am forever grateful for your **unconditional** love.

Abstract

In 2020, prostate cancer (PCa) was the fifth major cause of cancer mortality in individuals assigned male at birth (AMAB). The current strategy to combat PCa is regular screening for early detection, since the cancer is often asymptomatic during early stages, where chances of survival are greater. However, the current clinical management of PCa relies on an observational, population-based paradigm, which does not enable to adapt clinical care to relatively latent, less aggressive tumours from fast-growing, life-threatening ones. Hence, patients frequently undergo over- or undertreatment, resulting in an unnecessary loss of quality of life.

Despite the considerable progress in PCa grading, diagnosis, and treatment strategies the design of patient-specific optimal management plans is very limited nowadays. However, the use of mathematical oncology techniques can personalize PCa care by optimizing therapeutic or monitoring regimens *in silico* and, hence, contribute significantly to solve the problem of over- and under-treatment.

In this context, this thesis presents a mathematical model to explore the roles of the prostate's ductal structure in the progression of PCa during its early stage, and how this leads to the formation of different Gleason patterns (GPs), which characterize PCa aggressiveness and are central to the identification of high-risk disease. The model leverages the phase-field method to represent the tumour and the prostatic ducts, along with a set of reaction-diffusion equations to describe the dynamics of key substances driving the development of the disease (e.g., nutrient, matrix metalloproteinases (MMPs)). In this work, we perform a computational study in a 2D tissue patch in which we explore how variations of the model parameters change PCa dynamics, with particular focus to tumour branching and the degradation of the extracellular matrix (ECM) that makes up the ductal structure.

Resumo

Em 2020, o cancro da próstata (PCa) foi a quinta principal causa de mortalidade por cancro em indivíduos designados homem ao nascer (AMAB). A estratégia atual para combater o PCa é a triagem regular para deteção precoce, uma vez que o cancro é frequentemente assintomático nas fases iniciais, onde as chances de sobrevivência são maiores. No entanto, atualmente o tratamento clínico do PCa baseia-se num paradigma observacional baseado na população, que não permite adaptar os cuidados clínicos a tumores relativamente latentes e menos agressivos em comparação com aqueles de rápido crescimento e potencialmente fatais. Como resultado, os pacientes são frequentemente submetidos a tratamentos excessivos ou insuficientes, resultando numa perda desnecessária de qualidade de vida.

Apesar dos consideráveis avanços na classificação, diagnóstico e estratégias de tratamento do PCa, atualmente o desenvolvimento de um plano de tratamento otimizado e específico para cada paciente permanece limitado. No entanto, a utilização de técnicas da oncologia matemática pode personalizar o tratamento do PCa ao otimizar planos terapêuticos ou de monitorização *in silico*, contribuindo significativamente para resolver o problema do tratamento excessivo ou insuficiente.

Neste contexto, esta tese apresenta um modelo matemático para explorar os papéis da estrutura ductal da próstata na progressão do PCa durante a sua fase inicial e a consequente formação de diferentes padrões de Gleason (GPs), que caracterizam a agressividade do PCa e são fundamentais para a identificação de doença de alto risco. O modelo utiliza o método de phase-field para representar o tumor e os ductos prostáticos, bem como um conjunto de equações de reação-difusão para descrever a dinâmica de substâncias-chave que impulsionam o desenvolvimento da doença (e.g., nutrientes, metaloproteinases da matriz (MMPs)). Neste trabalho, realizamos um estudo computacional num *patch* de tecido 2D em que exploramos como variações nos parâmetros do modelo alteram a dinâmica do PCa, focandomo-nos particularmente na ramificação do tumor e na degradação da matriz extracelular (ECM) que compõe a estrutura ductal.

to use a metaphor
at a time like this
would be obscene.

Philip Hodgins

Contents

List of Figures

List of Tables

Acronyms

ABP	Acute bacterial prostatitis
ADAM	A disintegrin and metalloprotease
AFS	Anterior fibromuscular stroma
AIP	Asymptomatic inflammatory prostatitis
AMAB	Assigned male at birth
BPH	Benign prostatic hyperplasia
CBP	Chronic bacterial prostatitis
CSPC	Clinically significant prostate cancer
CSC	Cancer stem cell
CT	Computerized tomography
CZ	Central zone
DRE	Digital rectal examination
ECM	Extracellular matrix
EMT	Epithelial to mesenchymal transition
GP	Gleason pattern
GS	Gleason score
ISUP	International Society of Urologic Pathology
MMP	Matrix metalloproteinase
MMPI	Matrix metalloproteinase inhibitor

MT-MMP	Membrane-type matrix metalloproteinase
MRI	Magnetic resonance imaging
NICD	Notch intracellular domain
PBC	Periodic boundary condition
PCa	Prostate cancer
PDE	Partial differential equation
PET	Positron emission tomography
PIN	Prostatic intraepithelial neoplasia
PIA	Proliferative inflammatory atrophy
PSA	Prostate-specific antigen
PZ	Peripheral zone
TIMP	Tissue inhibitors of metalloproteinase
TRUS	Transrectal ultrasound
TSG	Tumour suppressor gene
TZ	Transition zone
VEGF	Vascular endothelial growth factor

List of Symbols

Main Variables

Symbol	Description
ϕ	Tumour phase-field
σ	Nutrient
ψ	Duct phase-field
C_M	MMP concentration
ρ	MMP phase-field
t	Time

Main Parameters

Symbol	Description	Units
D_ϕ	Diffusivity of the phase-field (tumour)	$\mu\text{m}^2 \cdot \text{d}^{-1}$
τ	Interface relaxation time	d
χ	Nutrient-driven growth	$g \cdot L^{-1} \cdot \text{d}^{-1}$
A	Apoptosis rate	d^{-1}
D_σ	Nutrient diffusivity	$\mu\text{m}^2 \cdot \text{d}^{-1}$
s	Nutrient supply	$g \cdot L^{-1} \cdot \text{d}^{-1}$
δ	Nutrient consumption rate	d^{-1}
Nutrient decay rate	d^{-1}	
D_ψ	Diffusivity of the phase-field (duct)	$\mu\text{m}^2 \cdot \text{d}^{-1}$
τ_D	Interface relaxation time	d
μ	Duct's resistance to infiltration	—
η	Tumour vs. duct interface ratio	—
$\hat{c}$	Interface curvature	μm^{-1}
$\hat{n}$	Normal vector to the contour surfaces of ψ	μm
D_{C_M}	MMP diffusivity	$\mu\text{m}^2 \cdot \text{d}^{-1}$
α	MMP production coefficient	d^{-1}
ζ	MMP degradation coefficient	d^{-1}
k	MMP concentration where $f(C_M) = 0.5$	—
n	Hill coefficient	—
M_ρ	Mobility of order parameter ρ	d^{-1}
Γ^+	Forward reaction rate coefficients	d^{-1}
Γ^-	Reverse reaction rate coefficients	d^{-1}

Chapter 1

Introduction

Understanding cancer biology and behaviour is critical for creating effective cancer preventive and treatment strategies. Mathematical models have become a significant tool in cancer research, aiding treatment outcome predictions and elucidating underlying mechanisms. This chapter will provide an outline of the thesis' objectives (**Section 1.1**), motivation (**Section 1.2**), state of the art in mathematical modelling of prostate cancer (PCa) research (**Section 1.3**), and lastly a thesis overview (**Section 1.4**).

1.1 Objectives

This work is part of a larger research whose goal is to develop a phase-field mathematical model of the early development of PCa aims at providing insights into the mechanisms underlying tumour growth, which can aid in the development of personalized treatment plans, in order to minimize over- and undertreatment.

The purpose of this thesis is to build a PCa model to investigate the early phases of tumour development, the establishment of distinct Gleason Patterns (GPs), and provide insight into how different parameters affect the growth and progression of the tumour.

1.2 Motivation

In 2020, PCa was the second most commonly diagnosed cancer and the fifth major cause of cancer mortality in individuals assigned male at birth (AMAB), with an approximate 1.4 million new diagnoses and 375 000 deaths globally [1]. Worrisomely, after two decades of reduction, cancer incidence for PCa rose by 3% yearly from 2014 to 2019, according to the American Cancer Society, which estimates 288 300 new cases and 34 700 deaths in 2023, in the USA alone [2].

Prevention and routine screening for early detection are the present strategies used to battle

PCa, since there is a favourable survival rate for localized PCa. Conversely, the likelihood of a precise prognosis declines in later stages, namely because of difficulty in diagnosing metastatic events in PCa progression [3].

However, the notion that cancer screening increases the probability of eliminating and treating cancer lesions is an ambiguous one, with multiple studies reaching contradictory conclusions on whether serum prostate-specific antigen (PSA) screening is beneficial, since it was first introduced in 1991 [4]. Distinguishing between true positives and false positives often implies individuals to undergo potentially dangerous procedures such as biopsies, as well as treatment for less aggressive, slow-growing tumours. Thus, PSA screening has been suggested to be a main driver of overdiagnosis and overtreatment, resulting in an unnecessary loss of quality of life [5]. Despite the considerable progress in PCa grading, diagnosis and treatment strategies made, more research is needed to fully understand the fundamental mechanisms of cancer progression and GP formation, if we want to decrease mortality rates.

To address the current excesses and deficiencies in PCa patient treatment and gain insight in the underlying biology of its pathological progression, mathematical oncology offers the possibility to investigate PCa growth mechanisms and optimal treatment planning *in silico*. Indeed, it has been argued that PCa is an ideal choice for implementing tissue-scale mathematical modelling. The prostate gland is small, and has a relatively simple geometry, facilitating the development of a mathematical model that accurately represents gland geometry and tumour growth. Additionally, PCa is a slow-growing cancer, which allows for the collection of comparably larger patient-specific longitudinal data than for other tumours. Then, these larger datasets are a pivotal asset that can be used for model calibration as well as for validation of model predictions. In particular, PSA levels have been extensively used to calibrate and validate mathematical models of PCa growth and treatment response, as this biomarker is ubiquitously used in the management of the disease [6]. All these features contribute to the possibility to study the tumour's growth in isolation as well as its interactions with the surrounding tissue. Nevertheless, it is important to keep in mind that existing models are still simplifications of a complex biological system whose mechanisms are yet to be fully deciphered.

1.3 State of the art

To date, modelling efforts have made use of a wide scope of model types and methodologies (based on biophysical, statistical, and empirical formulations) to explore certain essentials about the development of PCa and the effectiveness of its treatments.

From initial observation-driven approaches to data-validated models, as a consequence of

technological advances and increasing availability of clinical and experimental data, the field of computational oncology in PCa has been steadily advancing, with numerous studies utilizing mathematical models and simulations to improve our understanding of the disease [7].

Yorke *et al.* (1993) [8] is attributed with the first mathematical model of PCa progression, which is based on Gompertzian growth to explore the metastasis process and how it affects treatment efficacy. Mathematical models featuring multiple cell types such as this pioneering work became popular [9, 10, 11, 12, 13, 14, 6], since describing interactions between the different sub-population of cells proved to be a great tool for not only studying tumour growth, but also exploring different types of hormonal therapy. Because this type of therapy is the benchmark of treatment for metastatic PCa, several models have been created in an effort to grasp how different drugs influence tumorigenesis. Particularly, kinetic-type models have successfully replicated drug effects on the dynamics of androgen based on pharmacokinetics models [15, 16, 17, 18]. Such models may offer limited computational tractability and have been further developed over time, addressing issues of complexity using multi-level fitting to facilitate parameter estimation [19] or simplifications [20] as well as by adding compartments to study multi-drug therapy [21]. Immunotherapy has also been explored in the setting of mathematical modeling of PCa, including studies in: combination therapy [22], effectiveness of dosage and treatment [23] or even prediction of treatment failure time [24].

As previously mentioned, an important clinical parameter frequently used in model validation is serum PSA, as it is the most common biomarker for PCa growth [25, 26, 27, 6, 28]. But are serum PSA levels a robust and accurate way to track tumour progression and malignancy? Different models have explored this question, as well as other alternative PSA metrics (such as PSA relative velocity), or combining PSA with other supplementary clinical measurements (like patient Gleason score (GS)) [29, 30, 31, 32].

The majority of mathematical models describing PCa growth and treatment response only account for the temporal dynamics of these phenomena by leveraging one or several ordinary differential equations. However, there is a dearth of spatially-resolved mathematical models representing the mechanisms underlying PCa progression and the effects of therapies. Importantly, spatial, memory-based, and stochastic models will be helpful in identifying spatial patterns in tumour growth and interplay, including the metastatic processes, as more data, particularly imaging data, becomes available [7].

In general, the development of the mathematical models outlined in this section signifies an improvement in our knowledge of PCa and its management. Specifically, these models can provide insight into the biological processes involved in PCa progression and treatment efficacy

and, therefore, they can also contribute to create more efficient methods for diagnosis, prognosis, and therapy by employing mathematical and computational techniques to capture the intricate dynamics of tumour growth and invasion. Hence, in order to enhance patient outcomes, the state of the art in PCa computational oncology is centred on creating personalized, predictive models that use data from multiple sources (e.g., PSA, medical imaging).

1.4 Thesis overview

After this introduction, Chapter 2 of this thesis presents a summary of current information that serves as the framework for the research described in this work. This chapter discusses the characteristics of the prostate, and the molecular mechanisms of PCa as well as its standard diagnosis and treatment. In Chapter 3, we propose a continuous model that simulates the growth patterns of localized PCa using a phase-field approach based on nutrient dynamics.

Then, Chapter 4 provides the results of a computational study of the model and a discussion of the main findings. Finally, Chapter 5 summarizes the thesis and its contributions, as well as future study directions. For the reader's convenience, the bibliography is included at the end of this document.

Chapter 2
Biological Background

In the present chapter we focus on the biological context that provides the basis for the work presented herein. We begin with an overview of the cancer mechanisms (**Section 2.1**), the prostate and its anatomy, histology, and physiology, as well as common pathologies of the human prostate (**Section 2.2**). Next, we focus on the mechanisms involved in the development of PCa itself, its diagnosis, and its grading depending on the architectural structure of the tumour (**Section 2.3**). Finally, we explore the mechanisms involved in the progression of PCa, with special focus on the roles of matrix metalloproteinases (MMPs) and the Notch signalling pathway (**Section 2.4**).

2.1 Understanding cancer

Cancer is usually characterized by an aberrant, excessive level of net proliferation that stems from an imbalance of cell proliferation and death processes. Simply put, tumour cells do not respond to the control mechanisms put in place by the host tissue. Most often, this process of carcinogenesis occurs due to accumulation of genetic alterations, such as a genetic mutation or epigenetic modification taking place in the cell's DNA, and leading to the overexpression of an oncogene (which promotes cell cycle progression) or, equally, the underexpression of a tumour suppressor gene (TSG, which inhibits the cell cycle). Additionally, some genetic alterations may enable precancerous and cancerous cells to bypass DNA repair mechanisms, which makes the cell and its descendants to be more susceptible to the acquisition of further mutations and epigenetic changes which may enable them to become enable it "immortal" due to the imbalance between growth and inhibitory signals. Less commonly, these mutations can arise not from direct genetic alteration of a cell or group of cells, but from induction of changes in gene expression, for example, due to microenvironmental signals or even viral infection [33]. Furthermore, carcinogenesis can be and is often exacerbated by external factors such as the individual's lifestyle and their environment (like exposure to carcinogenics) (see [34]). Thus,

the hallmarks of cancer (Figure 2.1) include self-sufficiency in growth signals, insensitivity to growth-inhibitory signals, evasion of programmed cell death (apoptosis), limitless replicative potential, sustained angiogenesis, and tissue invasion and metastasis, which is the process where the tumour grows and spreads to nearby tissues and organs [35].

There are several hundred distinct neoplastic malignancies from a histology perspective, which are divided into six main categories: carcinoma, sarcoma, myeloma, leukaemia, lymphoma, and mixed types. We focus on carcinomas, which are the most common type of cancers (80% to 90% of all cancer cases), and develop in epithelial tissues (i.e. tissue that lines the inner or outer surfaces of the body). Adenocarcinomas, which develop in an organ or gland, and squamous cell carcinomas, which arise in the squamous epithelium, are the two main kinds of carcinomas. The majority of carcinomas develop in glands or organs capable of secretion, including the prostate [36].

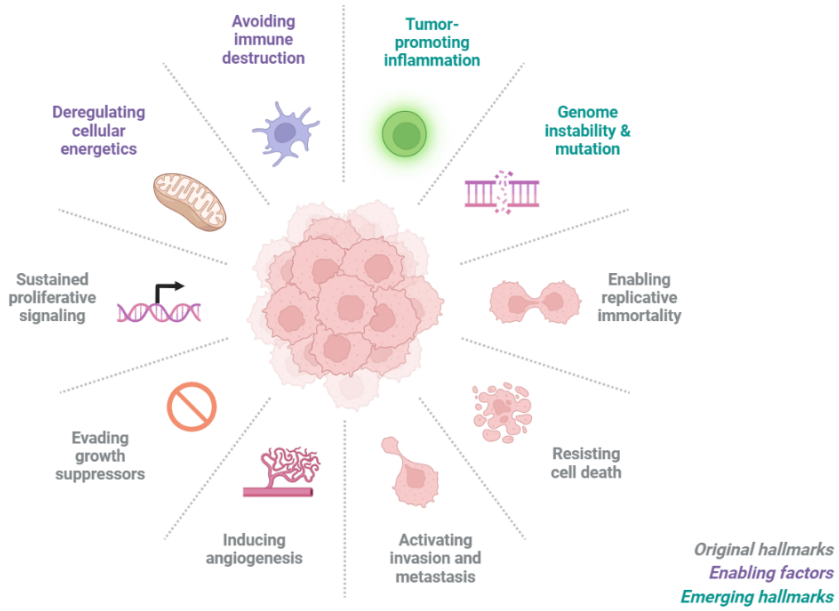

Figure 2.1: **The hallmarks of cancer**. Adapted from [35].

2.2 The prostate

2.2.1 Anatomy, histology and physiology of the human prostate

The human prostate is a small glandular organ, whose geometry is often described as an inverted cone. The volume of the prostate in young healthy individuals is usually 21 cc, but its volume increases with age and may reach and exceed 100 cc in elderly individuals. It is located just below the urinary bladder and in front of the rectum, surrounding the urethra, with the

seminal vesicles located bilaterally at the base of the gland (Figure 2.2) [37]. McNeal *et al.* [38, 39] first described the anatomy of the prostate, dividing it into an anterior fibromuscular stroma (AFS) zone and three glandular zones: peripheral zone (PZ), transition zone (TZ), and central zone (CZ). As portrayed in Figure 2.3, the PZ is the largest zone, making up 70% of tissue in the prostate, and is where most PCas develop. In most young individuals, the TZ makes up around 5% of the prostate and is situated close to the prostatic urethra. However, benign prostatic hyperplasia (BPH), an exceedingly frequent pathology in older men, causes the TZ to expand significantly in the majority of older individuals. Tumours can also develop in the TZ, and there is evidence that there are physiological distinctions between these and the ones that develop in the PZ. The CZ makes up 25% of the prostatic tissue in healthy individuals and surrounds the ejaculatory ducts. Finally, the AFS is a thick, non-glandular band that forms the anterior surface of the prostate [40].

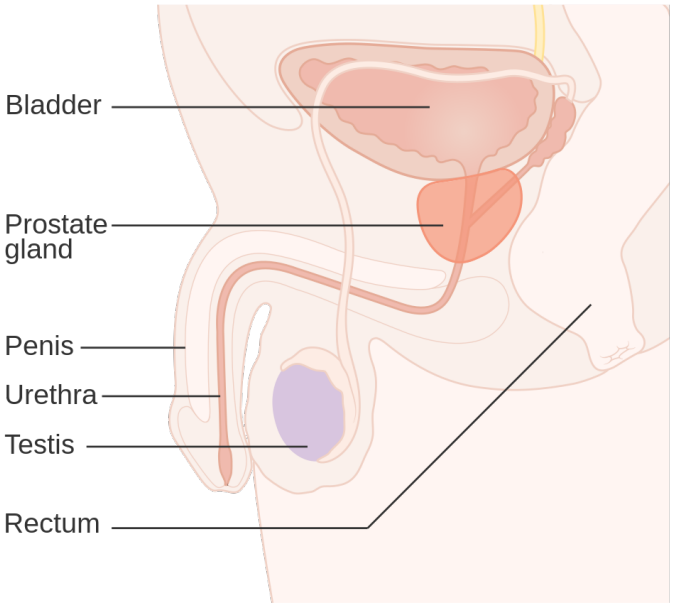

Figure 2.2: **Diagram of a sagittal cross-section of the pelvis** showing the anatomic position of the prostate. Provided by Cancer Research UK [41].

The glandular tissue is arranged into tubuloalveolar units, which are composed of acini and ducts that are lined by the epithelial cells. Histologically, the human prostate presents two main cell types: stromal and epithelial. Additionally, there are three types of epithelial cells: basal, luminal and neuroendocrine, which form the prostatic ducts and are embedded in the fibromuscular stroma (Figure 2.4) [43, 44, 45]. Secretory luminal cells, a differentiated androgen-dependent cell type that produces prostatic secretory proteins, are the most common

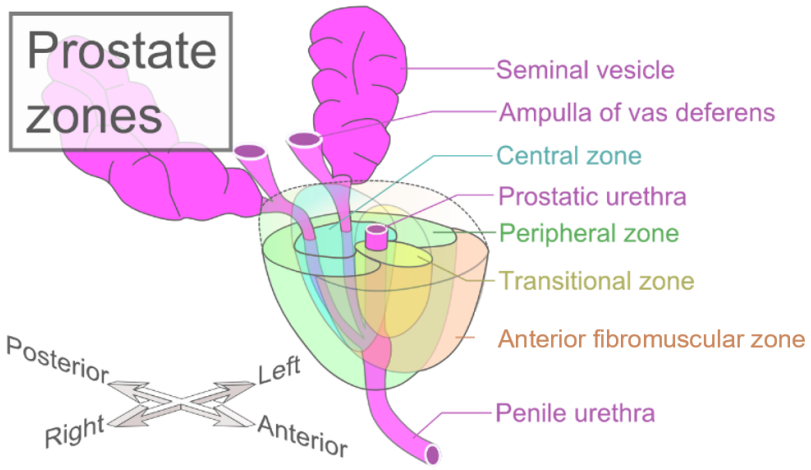

Figure 2.3: **Zonal anatomy of the human prostate**. Public Domain image adapted from [42].

cell type. The basal cells, which make up a continuous layer in the human prostate that lies between luminal cells and the basal lamina, are the second main epithelial cell type. Basal cells lack secretory capabilities.

The primary function of the prostate is the secretion of fluid which becomes part of the semen. Indeed, the majority of the seminal fluid is composed of secretions produced by the prostate and the seminal vesicles. Acid phosphatase, amylase, zinc, fibrinolysin, and PSA are all present in the mildly acidic secretions of the prostate [37].

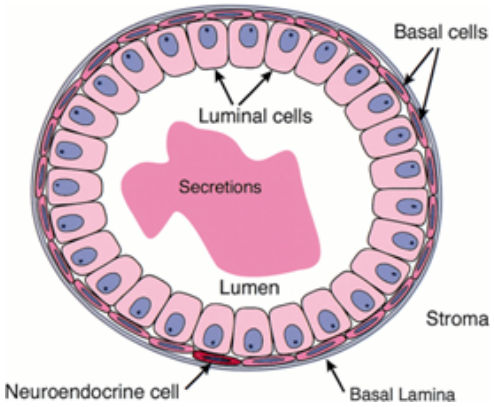

Figure 2.4: **Schematic representation of a prostatic duct** showing bilayered epithelium composed of the luminal layer and the basal layer consisting of small cuboidal cells. Adapted from [43].

2.2.2 Pathology of the human prostate

Prostatitis, BPH, and PCa are the most prevalent prostate diseases. Prostatitis, which is the inflammation of the prostate gland, is the third most prevalent urogenital condition in males and in people AMAB after BPH and PCa [46, 47]. Prostatitis, in contrast to these two disorders which primarily affect older people, affects individuals of all ages, but especially those in the middle age group. Additionally, there are several subtypes of prostatitits, namely acute bacterial prostatitis (ABP), chronic bacterial prostatitis (CBP), chronic prostatitis/chronic pelvic pain syndrome, and asymptomatic inflammatory prostatitis (AIP) [48].

BPH, as previously established, refers to the nonmalignant growth of the prostate that occurs in the TZ. The histologic prevalence of BPH is approximately 10% for men in their 30s, 20% for men in their 40s, 50% to 60% for men in their 60s, and 80% to 90% for men in their 70s and 80s. Thus, this disorder occurs as an age-related phenomenon in virtually all individuals AMAB [49, 50]. Lastly, PCa is the most serious prostate pathology, and will be discussed more extensively in the following section.

2.3 Prostate cancer

The vast majority of PCa cases are adenocarcinomas, which means that the tumour originates from the glandular cells of the prostate. It is typically a disease that affects older individuals AMAB, with 6 out of 10 cases being identified in patients 65 or older with a mean age of approximately 66 at the time of cancer diagnosis [51]. The probability of acquiring PCa rises with age, from 0.005% in individuals under the age of 39 to 2.2% in those between 40 and 59, and 13.7% in those between 60 and 79 [52]. In 2020, it was responsible for approximately 1.4 million new diagnoses and 375 000 deaths across the world [1].

2.3.1 Origin and progression

For a disease as common as PCa, relatively little is known about its aetiology. Despite this, some risk factors have been suggested such as: age, ethnicity, family history, genetics, obesity, diet, hormones, smoking, alcohol, and some medications. Excluding ethnicity and age, none of these factors have been definitively established as contributing factors [52].

On a cellular level, PCa is characterised by a dysfunctional differentiation of the normal epithelial lineage, resulting in luminal hyperproliferation, loss of the basal cell layer, breakdown of the basal lamina, immune cell infiltration and stromal reactivity [53]. The cellular origin of PCa is a heavily debated topic: although the most reported PCa is acinar adenocarcinoma

(arising from the prostate gland secretory luminal lineage), it has been proposed that while luminal cells are favoured as cells of origin in many contexts, basal cells can also give rise to tumours after differentiating into luminal cells. Furthermore, a smaller subset of PCa develops from the neuroendocrine cell lineage, originating what is called small cell-carcinoma [45, 54].

Currently, there are two hypotheses for the development of the dysfunctional differentiation at PCa onset [53]: (i) the stochastic model, and (ii) the cancer stem cell (CSC) model. In the stochastic model, there must be an event that affects the expression of an oncogene or a TSG in one cell, ensued by mitosis that produces an equally mutated cell. PCa then results of the accumulation of genetic defects in the descendants of the starting cell [55]. The CSC hypothesis postulates that only a small subpopulation of cancer cells within a tumour has the capacity to generate the tumour. This pool of cells, CSCs, is capable of self-renewal, and is highly proliferative, meaning it would be responsible for the dysregulated differentiation from which PCa originates. It is thought that these models are not mutually exclusive, and perhaps play different roles at different stages of PCa development [53, 56].

The exact molecular mechanisms underlying prostate carcinogenesis and progression remain elusive. Even so, there seems to be a multistage developmental progression from healthy tissue to preneoplastic lesions (Figure 2.5), which the lead to full-fledged invasive adenocarcinoma of the prostate and eventually androgen-independent lethal disease. The preneoplastic conditions include proliferative inflammatory atrophy (PIA) and proliferative inflammatory neoplasia (PIN). The proposed model hypothesises that some form of inflammatory damage is responsible for PIA, which has been demonstrated to mix with regions of PIN and malignant tissue, connecting and reinforcing the idea of a sequential development of carcinogenesis [57, 58, 59, 60].

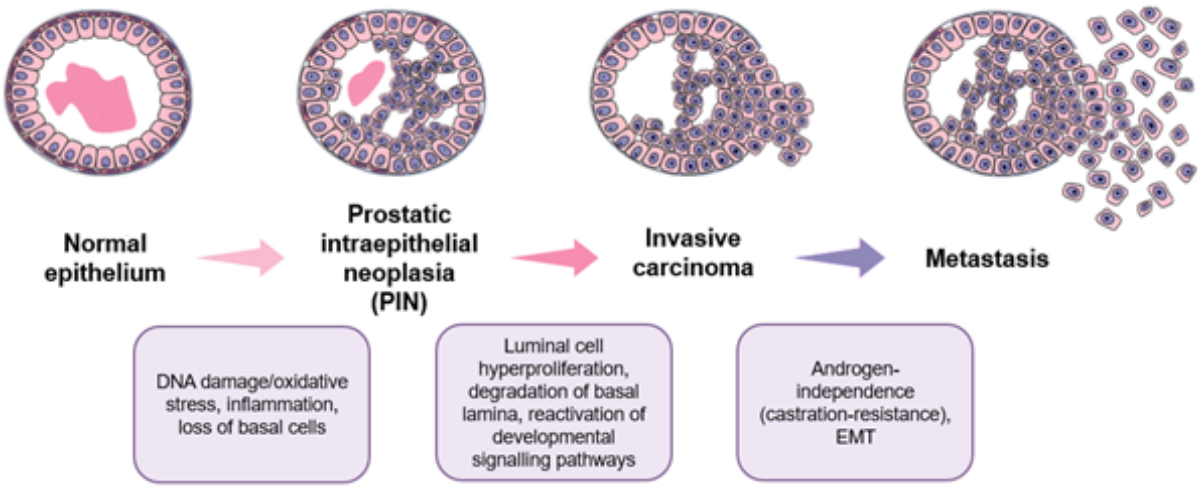

Figure 2.5: **Progression pathway for human PCa**, and the different molecular processes associated. Adapted from [43].

2.3.2 Diagnosis

Because PCa often produces little to no symptoms in its early stages, currently the strategy used to tackle PCa is prevention and screening (recommended to men and people AMAB over age fifty [45]) to optimize early detection and possible treatment [61]. Since PCa is a heterogeneous disease (from small latent tumours to metastatic cancer), it is important that clinicians can determine the aggressiveness, the location and extension of the cancer in order to guide treatment.

Typically, PCa is diagnosed via digital rectal examination (DRE), evaluation of PSA level in blood, and transrectal ultrasound (TRUS) guided biopsy, which is considered the gold standard method of diagnosis because it provides histopathological confirmation of the disease. The DRE involves a doctor inserting a gloved finger into the rectum to feel the prostate for firm lumps or other abnormalities. Suspicious DRE results are associated with higher risk of clinically-significant prostate cancer (CSPC) in patients with high PSA values, and the test has less significancy in patients with normal PSA levels [62]. The PSA test is a blood test that measures the serum level of this prostate activity biomarker, which is associated with an increased risk of PCa. Still, PSA is not cancer-specific, with abnormal values of PSA also being attributed to other pathologies such as BPH and prostatitis. While the standard threshold for PSA level is considered to be 4.0 ng/mL, urologists must take into consideration the context of the patient, like age, race, comorbidities and family history [63]. If screening tests suggest the presence of PCa, a TRUS-guided biopsy is usually performed, where small tissue samples are collected from the prostate and examined under a microscope to confirm the presence of cancer. If the presence of cancer cells is confirmed, a pathologist will then determine the tumour's aggressiveness, by microscopic observation of the prostatic tissue architecture [63].

Novel complementary screening and diagnosis methods are being researched, such as measuring the blood levels of matrix metalloproteinases (MMPs), which are enzymes that play a role in the breakdown of the extracellular matrix (ECM) [64]. MMP levels have been shown to be positively correlated with GS, which, in turn, is associated the aggressiveness of the cancer [64, 65, 66]. Medical imaging, such as ultrasound, magnetic resonance imaging (MRI) [67], or Choline C-11 positron emission tomography (PET) scan simultaneously with a low-dose computerized tomography (CT) scan, may also be used to detect PCa.

Gleason grading system

The Gleason grading system (Figure 2.6) was created in 1966 by pathologist Donald Gleason, and since adopted worldwide. This system aims at estimating the prognosis of PCa patients

by stratifying PCa based on its microscopic structure into groups of increasing aggressiveness [68, 69].

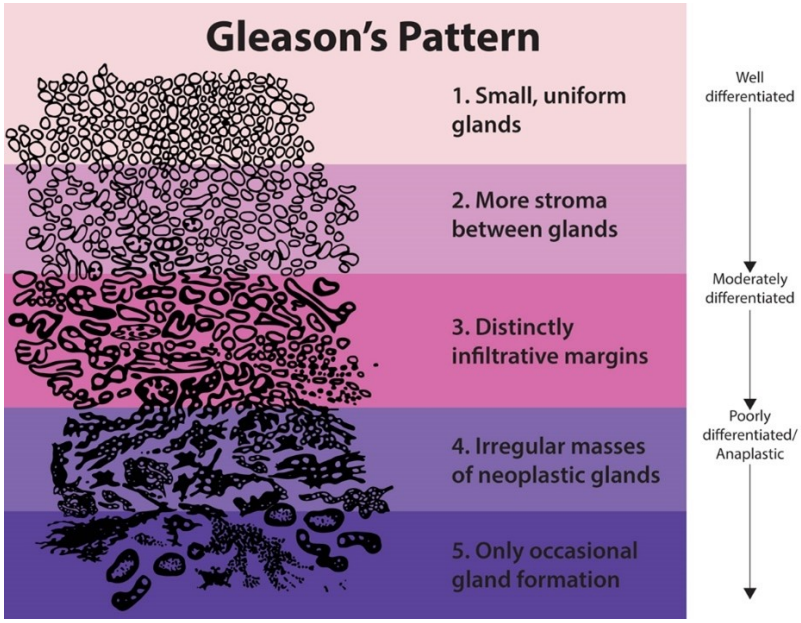

Figure 2.6: **Schematic depiction of the different Gleason Patterns**. Reproduced from [70].

Looking at PCa in haematoxylin and eosin-stained histology (H&E) slides histopathologists can identify five architectural GPs (also known as Gleason grades), corresponding to different levels of neoplastic progression. Each pattern is labelled with a number from 1 to 5, with higher patterns corresponding to more aggressive cancers and worse prognosis [71]. Then, the GS is calculated by summing the most and the second most prevalent patterns identified in the biopsy tissue, meaning that the GS ranges from 2 (1+1) to 10 (5+5). A summary description of each grade is presented in Table 2.1.

The Gleason grading system has been extensively shown to correlate with prognostic and therapeutic outcomes, even more so after the 2005 International Society of Urologic Pathology (ISUP) conference, which resulted in a Modified Gleason System, characterized by more detailed descriptions [72]. However, being a subjective evaluation, it has been proved that there exists high intra and inter-observer variability when grading PCa, as well as a lack of granularity [73, 74]. This means that if a patient showed a GS of 7, it often was not distinguished between being a result of a 3+4 score or a 4+3 score, despite these scores having different prognosis. To address the limitations of GS, a new grading system was developed, Grade Groups (Table 2.1), and accepted in the 2014 ISUP Consensus Conference on Gleason Grading of Prostatic Carcinoma as it proved that would prevent overtreatment. Currently, Gleason Grade Groups are used in conjunction with the Gleason grading system [75].

Table 2.1: **Summary description of the Gleason grades & Grade Groups**. From [69, 72].

Grade	Description
1	Simple round glands, close-packed in rounded masses with well-defined edges
2	Simple rounded glands, loosely packed in vague, rounded masses with loosely defined edges
3A	Medium sized single glands of irregular shape and irregular spacing with ill-defined infiltrating edges
3B	Very similar to 3A, but small to very small glands, which must not form significant chains or cords
3C	Papillary and cribriform epithelium in smooth, rounded cylinders and masses; no necrosis
4A	Small, medium, or large glands fused into chords, chains, or ragged, infiltrating
4B	Very similar to 4A, but with many large clear cells, sometimes resembling "hypernephroma"
5A	Papillary and cribriform epithelium in smooth, rounded masses, more solid than 3C and with central necrosis
5B	Anaplastic adenocarcinoma in ragged sheets
Grade Group	**Description**
Grade group 1	Only individual discrete well-formed glands
Grade group 2	Predominantly well-formed glands with lesser component of poorly formed/fused/cribriform glands
Grade group 3	Predominantly poorly formed/fused/cribriform glands with lesser (>5%) component of well-formed glands
Grade group 4	Only poorly formed/fused/cribriform glands, or predominantly well-formed glands and lesser component lacking glands, or predominantly lacking glands and lesser component of well-formed glands
Grade group 5	Lack gland formation (or with necrosis) with or without poorly formed/fused/cribriform glands

3D architecture

It is important to study the 3D architectures of the different GPs, since the same grade observed in the H&E histology slides can correspond to vastly different 3D architectures of the tubuloalveolar structure. These architectures are illustrated in Figure 2.7 and were described by Leenders *et al.* naming them based on their physical attributes. GP3 has tubules with local interconnections and may form a continuous network with both fused GP4 (with increased interconnections) and poorly formed GP4 (showing reduced tubular diameter and size). Additionally, the poorly formed GP4 architecture may also evolve into the GP5 cords architecture which shows even more decreased tubular diameter and size, until lumens disappear. The glomeruloid GP4 architecture is defined by intraluminal protrusions of epithelial cells in a background of GP3 tubules and can be deemed as the intermediate condition between the two structural groups represented in Figure 2.7: the structures in which most tumour cells are in contact with the stroma (i.e., GP3, fused GP4, poorly formed GP4, glomeruloid GP4, and cords GP5), and the ones where most of these cells are not in contact with the stroma (i.e., cribriform GP4 and solid GP5). Furthermore, cribriform GP4 and solid GP5 (with or without comedonecrosis) present serpentine layers of epithelial cells [76, 77, 78]. Interestingly, if a patient has GP4, the predominant architectural pattern present (i.e., fused, poorly formed, glomeruloid, or cribriform) is associated with substantially distinct prognosis [79]. In particular, the presence of a cribriform pattern has been shown to be a good predictor for metastasis after radical prostatectomy and for biochemical recurrence, having poorer prognostic outcomes when compared to other GP4 architectures [80, 81, 82].

2.3.3 Morphoregulatory factors

PCa is characterized by the gradual proliferation and infiltration of malignant cells within the prostate gland's tubuloalveolar structures. While genetic changes in the epithelium are often the driving force in adenocarcinomas, atypical paracrine interactions also play a determinant role in PCa [83]. Hence, PCa growth mechanisms entail complex interactions between cancer cells, the surrounding stromal microenvironment, and numerous signalling pathways. Importantly, these mechanisms contribute to the deformation and alteration of the prostate gland's natural tubuloalveolar architecture during PCa progression, as outlined in the previous section.

The prostatic stroma is composed not only of stromal cells, smooth muscle and ECM, but also of nerves and blood vessels. Combined with the different subtypes of epithelial cells and biochemical milieu of the tissue, these components form the prostate microenvironment and influence cancer progression [84]. Despite the fact that the stromal-epithelial interactions and

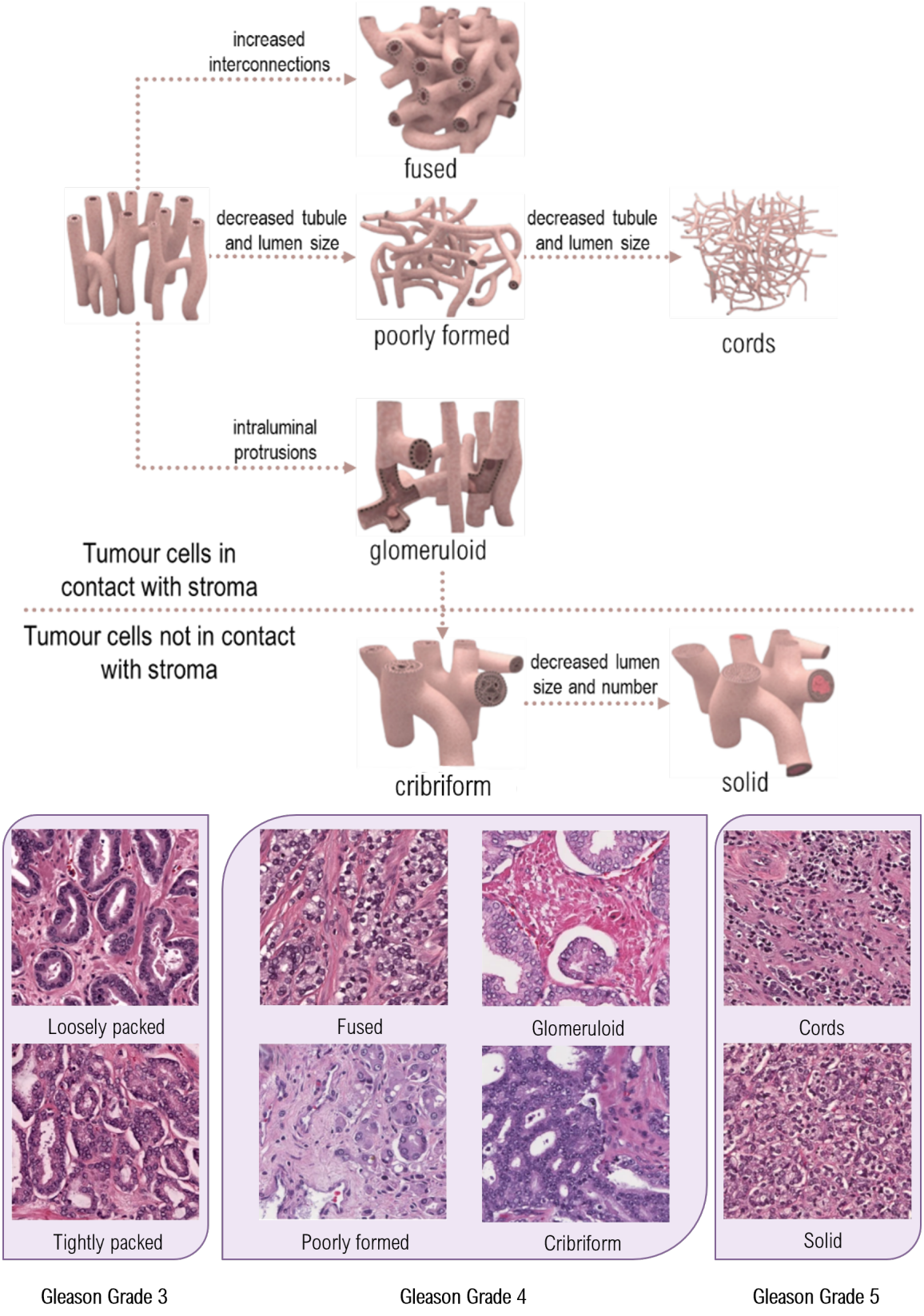

Figure 2.7: **Schematic overview of the Gleason growth patterns in PCa**, their 3D architecture, and corresponding H&E slides. Adapted from [73, 78].

molecular pathways involved in PCa carcinogenesis are similar to those involved in regular embryological development, these mechanisms are not as well understood in cancer as they are in normal embryogenesis. Specifically, pubertal prostates, PCa, and BPH gene expression profiles revealed shared gene expression patterns between the three cases. These findings emphasize the necessity of studying developmental pathways in BPH and PCa, as well as the possibility that numerous developmental pathways could be suitable targets for BPH and PCa therapy [85].

There are many morphoregulatory pathways in prostate ductal development that may contribute to the progression of PCa. These pathways have been shown to be essential for pathways which are essential for prostatic development initiation, budding, branching and differentiation [86]. Additionally, PCa progression has also been shown to be mediated by several other biological processes, such as the influence of the ECM in cell migration and proliferation, angiogenesis, and mechanisms involved in growth, invasion, and metastasis [87], like the ones regulated by MMPs. For the purposes of this work, we will focus individually on the Notch pathway and the roles of MMPs in PCa progression.

Matrix Metalloproteinases

Malignant tumours are distinguished by their ability to disrupt matrix barriers, allowing for invasion of adjacent tissues, intravasation, extravasation, and metastasis [88]. These phenomena are possible due to proteolytic systems capable of hydrolysing basic ECM components. Although several proteases have been linked to cancer spread, a particular family of enzymes known as MMPs have been the subject of considerable anticancer research [89]. These enzymes are zinc-dependent endopeptidases, they are named after their reliance on metal ions for catalysis and their capacity to destroy ECM structural proteins, and the are involved in typical hallmarks of cancer. In a paracrine way, cancer cells are able to stimulate surrounding host cells to produce MMPs, which can then be bounded on the cancer cell surface and used by them to induce the ECM degradation [90]. In humans, the MMP family consists of 23 enzymes that can be subdivided into six groups: collagenases (which degrade types I, II, and III collagen), gelatinases (which degrade type IV collagen), stromelysins (which degrade proteoglycans), matrilysins (which degrade several other ECM proteins), MT-MMP (which are membrane-type MMPs also capable of digesting ECM molecules), and other MMPs. For an overview on MMPs, the interested reader is referred to [91]).

MMP dysregulation boosts PCa progression into metastasis by disrupting the processes of morphogenesis, tissue repair, epithelial to mesenchymal transition (EMT), and angiogenesis [64]. Angiogenesis is the complex process of formation of new blood vessels and capillaries. In the

context of cancer, this process is mediated by growth factors released by cancer cells in regions of hypoxia or inflammation, such that the newly-formed blood vessels and capillaries facilitate the diffusion of nutrients and oxygen to those areas. During this process, the sprouting of endothelial cells to initiate the formation of the new blood vessel or capillary is mediated by MMPs, which enable the dismantlement of pre-existing endothelial-lined vessels. Additionally, angiogenesis is fundamental for tumour branching [92].

In the context of cancer, the role of MMPs is not only due to their direct action, but also to changes in the expression of their main regulators, which are termed tissue inhibitors of metalloproteinases (TIMP-1, TIMP-2, TIMP-3, and TIMP-4). Generally, in PCa, MMP activity is dysregulated due to an upregulation of MMPs and a loss of TIMP activity. MMPs are thought to be more active during the later stages of PCa given that they show higher expression in tumours with higher GS. Increased expression of MMP-2, -3, -7, -9, -13, -14, -15, and -26 has been reported in serum and tissue samples from PCa patients and is associated with advanced or metastatic stages, whereas MMP-1 expression is linked to lower grade carcinomas and a decreased incidence of invasion. In particular MMP-2 and -9 have been extensively researched, with studies indicating a link between increased activity and higher GS. The interested reader is referred to [64] for a summary of reported activity of MMPs in PCa).

Given the importance of MMP activity in cancer progression, these small enzymes could make excellent therapeutic targets. Because it was assumed that MMPs have a harmful role in tumour growth, synthetic matrix metalloproteinase inhibitors (MMPIs) have been developed and tested. However, due to toxicity at higher doses, this first-generation of these drugs failed in phase III studies [93]. MMP involvement in cancer progression has since been found to be less "black-and-white", with research revealing that some MMPs may have anti-cancer effects and, hence, emphasizing the importance of determining their activities in specific cellular contexts.

Notch Signalling Pathway

Notch signalling is initiated through the interaction between a cell surface receptor (Notch-1, -2, -3, -4), and its corresponding ligands found on neighbouring cells (Delta-like1, 3, 4 or Jagged-1, -2). Upon binding of the Notch receptor to its transmembrane ligand, the receptor undergoes proteolytic cleavage mediated by members of the A disintegrin and metalloprotease (ADAM) family as well as γ-secretase. Consequently, the Notch intracellular domain (NCID) fragment is released and translocated to the nucleus, where it exerts its regulatory influence on gene transcription [94].

The intricate and dynamic Notch pathway governs a diverse array of cellular activities, and

plays a fundamental role in normal prostate development. Furthermore, dysregulation of this pathway has been implicated in the initiation and progression of PCa, including tumour development, invasion, metastasis, and angiogenesis [95, 96]. Nevertheless, the functional significance of Notch signalling in PCa is controversial. While the literature agrees on the involvement of the Notch pathway in prostate development, different research groups regularly reach conflicting conclusions when researching its significance in PCa. Activation of this signalling cascade inhibited cancer growth in multiple studies [97, 98, 99], but others provided data that directly contradicted this impact [100, 101].

The "Goldilocks effect" could explain why both Notch pathway inhibition and activation suppress tumour progression. Moderate Notch signalling may promote growth, whereas high or low levels of pathway activation may inhibit growth, explaining these differences [102]. For example, in a study by Qing *et al.* (2020) that aimed to investigate Notch genes as potential biomarkers and drug targets using multidimensional analysis of multiple databases, it was highlighted how ambiguous this pathway is, having seemingly roles both as a tumour suppressor and a tumour promotor. Interestingly, from a clinical point of view, the authors found a positive correlation between GS and Notch-1 and Notch-4 expression, and that higher expression of Notch-1, Notch-3, and Notch-4 seemingly cause poor prognosis for PCa patients [103].

Therefore, more research needs to be conducted to unravel the mechanisms involved for the development of novel therapies targeting the Notch pathway in cancer in general, and in PCa, in particular.

Chapter 3

Methods

This chapter describes the computational model proposed in this master thesis. First, **Section 3.1** provides a brief overview of the phase-field method. Then, **Section 3.2** presents the mathematical model used for the work presented herein, and we delve into the specifics of how the **tumour**, **nutrient**, **prostatic ducts**, and **ECM degradation** are simulated.

3.1 The phase-field method

Phase-field models constitute a powerful computational framework for studying various physical phenomena. This modeling approach originated in the field of Physics, in the context of non-equilibrium systems in materials science. For example, the first applications of the phase-field method aimed at describing phase transitions and microstructural evolution, in the materials science field [104, 105]. Nevertheless, phase-field models have since extended to other fields, such as cell movement [106], dendritic growth [107], and tumour growth [108].

The main idea of this approach is that the state of the entire system is represented continuously by the order parameter, ϕ. The order parameter is a scalar field that varies between 0 and 1 (or -1 and 1), where $\phi = 0$ and $\phi = 1$ each represent a different phase, while intermediate values correspond a smooth interface between the two phases (Figure 3.1). Then, the spatiotemporal dynamics of the order parameter (i.e., the phase-field) are described by a set of unique PDEs. Thus, computer simulations of phase-field models enable the visualization of the evolving interfaces under different parameter settings [109, 110].

Taking into consideration that the mathematical framework of the phase-field model enables the description of complex spatial patterns and the evolution of interfaces, and that modern imaging techniques allow for tumour evolution tracking, it is reasonable to think that this modelling approach is well-suited for investigating and predicting spatio-temporal dynamics of tumours. Specifically, solid tumour growth can be seen as a moving boundary problem between healthy and cancerous tissue [111].

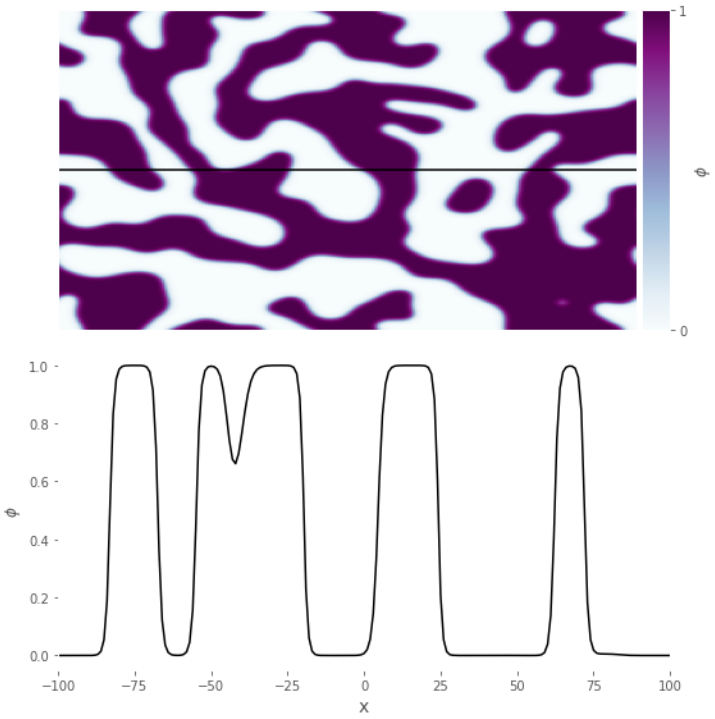

Figure 3.1: **Profile of order parameter (ϕ) on a line across the domain of a two-phase microstructure.**

3.2 Mathematical model

The model presented herein is an extension of the model developed by Lorenzo *et al.* [6], whose purpose was to define a tissue-scale, patient-specific computational framework that describes localized PCa growth. The model developed in this master thesis further includes the effect of the local geometry of prostatic ducts as well as the effect of MMP-mediated ECM degradation in PCa dynamics.

3.2.1 Tumour

We leverage the phase-field method to describe PCa growth as a moving boundary problem. Hence, we define an order parameter ϕ that jointly represents cancerous (ϕ=1) and healthy tissue (ϕ=0), while intermediate values define the evolving tumor interface (e.g., $\phi = 0.5$).

$$\phi = \begin{cases} 0, & \text{healthy tissue} \\ 1, & \text{tumorous tissue} \end{cases} \tag{3.1}$$

The derivation of the PCa growth model starts by defining a free energy function. We choose a Ginzburg-Landau free energy given by

$$E[\phi] = \int_{\Omega} \left(F(\phi) + \frac{\varepsilon^2}{2} (\nabla \phi)^2 \right) d\mathbf{r}, \tag{3.2}$$

where Ω denotes the spatial domain of the system, ϕ is the order parameter, and $\mathbf{r}$ is a position vector. The second term in the integrand of Eq (3.2) represents the surface energy, which is governed by the interface width ϵ. Additionally, F(ϕ) is a double-well potential, which is a function with two energy minima (0 and 1) that is provided by

$$F(\phi) = 16\phi^2(1-\phi)^2. \tag{3.3}$$

To describe PCa growth, we will use an Allen-Cahn phase-field formulation [112]. Hence, our model explains the temporal change of the order parameter in terms of the functional derivative of the free energy with respect to the order parameter, an interface relaxation time τ, and a series of reaction terms globally denoted by $R(\phi, \sigma)$ that depend on the order parameter ϕ and the local nutrient concentration σ. Thus, we can write the general formulation of our model of PCa growth as

$$\frac{\partial \phi}{\partial t} = -\frac{1}{\tau} \frac{\delta E}{\delta \phi} + R(\phi, \sigma), \tag{3.4}$$

To calculate the functional derivative of the free energy with respect to the order parameter, we first define

$$\delta E = E[\phi + \delta\phi] - E[\phi] = \int \frac{\delta E}{\delta \phi} \delta\phi d\mathbf{r}, \tag{3.5}$$

where

$$\begin{aligned} E[\phi + \delta\phi] = E[\phi] + \delta E &= \int \left(F(\phi + \delta\phi) + \frac{\varepsilon^2}{2} (\nabla(\phi + \delta\phi))^2 \right) d\mathbf{r} \\ &\approx \int \left(F(\phi) + \frac{dF}{d\phi} \delta\phi + \frac{\varepsilon^2}{2} \left((\nabla\phi)^2 + 2\nabla\phi \cdot \nabla\delta\phi \right) \right) d\mathbf{r} \\ &= \int \left(F(\phi) + \frac{\varepsilon^2}{2} (\nabla\phi)^2 \right) d\mathbf{r} + \int \left(\frac{dF}{d\phi} \delta\phi + \varepsilon^2 \nabla\phi \cdot \nabla\delta\phi \right) d\mathbf{r}. \end{aligned} \tag{3.6}$$

Consequently, by reintroducing the final expression from Eq (3.6) back into Eq. (3.2), we obtain

$$\begin{aligned}\delta E &= \int \left(\frac{dF}{d\phi}\delta\phi + \varepsilon^2 \nabla\phi \cdot \nabla\delta\phi \right) d\mathbf{r} \\ &= \int \left(\frac{dF}{d\phi} - \varepsilon^2 \nabla^2\phi \right) \delta\phi d\mathbf{r}.\end{aligned} \tag{3.7}$$

Finally, from Eqs. (3.5) and (3.7) we get

$$\frac{\delta E}{\delta \phi} = \frac{dF}{d\phi} - \varepsilon^2 \nabla^2 \phi \tag{3.8}$$

By bringing Eq. (3.8) back in to Eq. (3.5)), setting $D_\phi = \frac{\epsilon^2}{\tau}$, and introducing the formulation of the reaction terms for the model used herein, we arrive at the PDE describing PCa growth

$$\frac{\partial \phi}{\partial t} = D_\phi \nabla^2 \phi - \frac{1}{\tau}\frac{dF(\phi)}{d\phi} + \chi\sigma\phi - A\phi. \tag{3.9}$$

In Eq. (3.9), the term $\frac{dF(\phi)}{d\phi}$ is obtained straightforwardly from the double-well potential in (3.3) as

$$\frac{dF(\phi)}{d\phi} = 64\phi(\phi - 1)\left(\phi - \frac{1}{2}\right) \tag{3.10}$$

Additionally, the first reaction term in the right-hand side of Eq. (3.9) describes tumor cell proliferation as a nutrient-driven process governed by the proliferation rate χ and that depends linearly on the presence of cancer cells (ϕ) and the local nutrient concentration (σ). The second reaction term represents tumor cell apoptosis, which depends linearly on the order parameter (ϕ) and an apoptosis rate A. While the formulation of the proposed phase-field follows that of Lorenzo *et al.* [6], notice that the proliferation rate further depends on the order parameter instead of only on the local nutrient concentration.

3.2.2 Nutrient

While the proliferation of the tumour is a complex process where growth factors, androgen hormones, nutrients, and oxygen play a part, for the sake of simplicity we assume that tumour growth depends on the concentration of a generic nutrient, σ. We model the spatiotemporal dynamics of this generic nutrient with a reaction-diffusion PDE given by

$$\frac{\partial \sigma}{\partial t} = D_\sigma \nabla^2 \sigma + s - \delta\phi - \gamma\sigma. \tag{3.11}$$

In Eq. (3.11), the diffusion of the nutrient is governed by a diffusivity D_σ and it occurs from the local blood vessels and capillaries present in the prostate to the tissue. Hence, notice that the nutrient is not equally and readily available at all points of tissue. The first reaction term in the right-hand side of Eq. (3.11) represents the nutrient supply (s), which is modeled as discrete circular sources based on the average vascular density and diameter of blood vessels and capillaries in the prostate [113]. The last two terms respectively represent the consumption of nutrient by the tumor at a rate δ and the natural degradation of the nutrient at a rate γ. Additionally, it is also assumed that convection has a negligible contribution to glucose transport (i.e., that the bulk fluid flow on the movement of glucose is assumed to being insignificant compared to diffusion).

Given that the nutrient diffusion is much faster than tumor development (i.e., $D_\sigma \gg D_\phi$), Eq. (3.11) can be evaluated at equilibrium (a change added to the model implemented by Morais [114]). This assumption further facilitates the numerical resolution of the model during computer simulations by reducing the computational resources and time.

3.2.3 Prostatic ducts

As discussed in the **3D architecture** subsection, tumour growth influences the underlying ductal structure that makes up the prostate gland, and vice-versa. This process is not completely understood, although there are mechanisms known to contribute to it, as seen in the **morphoregulatory factors** section. To study the ducts' influence in tumour progression we introduce a new order parameter ψ that is dependent on the local morphology, such that $\psi = 0$ represents the duct and $\psi = 1$ corresponds to the neighboring stroma around the duct.

First, we need to extend the PDE governing PCa growth to include the effect of local morphology described by the new order parameter ψ. Towards this end, we extend the free energy introduced in Eq. (3.2) as follows:

$$E[\phi] = \int_\Omega \left(F(\phi) + \frac{F(\psi)}{\eta} + \mu\tau G(\phi,\psi) + \frac{\varepsilon^2}{2}(\nabla\phi)^2 + \frac{\varepsilon^2}{2}\frac{(\nabla\psi^2)}{\eta}) \right) d\mathbf{r}. \tag{3.12}$$

In Eq. (3.12), the parameter η lowers the energy associated with the duct's interface, overall reducing the surface tension contribution to the system. Furthermore, parameter μ regulates the influence of the duct. For higher values of μ, more energy is needed for the tumour to invade the tissue, such that its development will be more restricted within the duct geometry. For lower values of μ, the opposite holds true. Additionally, the term $\mathrm{G}(\phi,\psi)$ is given by

$$G(\phi,\psi)=\frac{\psi^2(2\psi-3)\phi^2(2\phi-3)}{2}. \tag{3.13}$$

Equation (3.13) is null when $\phi=0$ and $\psi=1$, and also when $\psi=0$. Thus, it reduces the system's energy when the tumour is inside of a duct, while increasing it when the tumour is outside of the duct. Following the same approach that rendered the PDE governing PCa dynamics from the free energy functional (i.e., Eqs. (3.3) and (3.9)), respectively), we can now use the extended free energy in Eq (3.12) to obtain the new model of PCa dynamics accounting for the underlying duct architecture as

$$\frac{\partial\phi}{\partial t}=D_\phi\nabla^2\phi-\frac{1}{\tau}\frac{dF(\phi)}{d\phi}+\chi\sigma\phi-A\phi-\eta\mu\frac{dG(\phi,\psi)}{d\phi}, \tag{3.14}$$

where,

$$\frac{dG(\phi,\psi)}{d\phi}=3\psi^2(2\psi-3)\phi(\phi-1). \tag{3.15}$$

Leveraging the same mathematical derivation followed to obtain the phase-field model governing PCa growth, we can also derive the PDE that describes the spatiotemporal changes to the duct architecture. This procedure requires using the functional derivative of the free energy with respect to order paramter ψ, and results in the following PDE:

$$\frac{\partial\psi}{\partial t}=D_\psi\frac{\tau}{\tau_D}\nabla^2\psi-\frac{1}{\tau_D}\frac{dF(\psi)}{d\psi}-\eta\mu\frac{\tau}{\tau_D}\frac{dG(\phi,\psi)}{d\psi} \tag{3.16}$$

where τ_D is the interface relaxation time, which is related to the mobility of the duct's wall. The lower the value of τ_D, the faster the duct deforms while the tumour is expanding. For higher values of τ_D and μ, the tumour will thus grow inside the duct, which will be rigid.

Because the duct's wall (or interface) introduces a surface-like energy that causes an interface contraction, Paiva [115] added a new term to counteract this effect, which is dependent on the curvature, as follows,

$$\frac{\partial\psi}{\partial t}=D_\psi\frac{\tau}{\tau_D}\nabla^2\psi-\frac{1}{\tau_D}\frac{dF(\psi)}{d\psi}-\eta\mu\frac{\tau}{\tau_D}\frac{dG(\phi,\psi)}{d\psi}+D_\psi\frac{\tau}{\tau_D}\hat{c}|\nabla\psi|, \tag{3.17}$$

where the interface curvature, $\hat{c}$, is given by,

$$\hat{c}=-\nabla\cdot\hat{\mathbf{n}}, \tag{3.18}$$

with $\hat{n}$ being the normal vector to the contour surfaces of ψ, and thus defined $\hat{n} = \nabla\psi/|\nabla\psi|$. This addition proposed by Biben *et al.* [116] as a phase-field approach for vesicle dynamics, guarantees that the interface movement is consequence of any imposed force and not of the interface surface tension.

3.2.4 ECM degradation

In order to study and simulate the changes of the normal tissue organization of the prostate during tumour growth that leads to the formation of different GPs, we need to model the ECM breakdown of the prostatic ducts, which allows the branching of the ductal structure, and tumour invasion of the tissue. To achieve this, we assume that this degradation process is primarily driven by the action of MMPs, which will act at the interface between the tumour and ECM. We will introduce a new non-dimensional variable C_M that represents the effect of the MMPs in degrading the ECM.

A singular source

Let us first assume that MMPs have a unique source, from which they diffuse into the prostatic tissue nearby. To model this case, we introduce a reaction-diffusion PDE that governs the spatiotemporal dynamics of local MMP concentration as follows

$$\frac{\partial C_M}{\partial t} = D_{C_M}\nabla^2 C_M + \alpha(\vec{r}) - \zeta C_M, \tag{3.19}$$

where $\alpha(\vec{r})$ is the production term for the MMPs, and ζ is the degradation coefficient. Here, the source of MMPs is considered to have a circular shape that will move to be at the interface between the tumour and the duct.

Given that MMPs degrade prostatic tissue, we can extend the phase-field model describing prostatic tissue architecture (i.e. Eq. (3.17)) as follows

$$\frac{\partial \psi}{\partial t} = D_\psi \frac{\tau}{\tau_D}\nabla^2\psi - \frac{1}{\tau_D}\frac{dF(\psi)}{d\psi} - \eta\mu\frac{\tau}{\tau_D}\frac{dG(\phi,\psi)}{d\psi} + \lambda\frac{\tau}{\tau_D}\hat{c}|\nabla\psi| - f(C_M)\psi, \tag{3.20}$$

where the MMP-driven degradation function $f(C_M)$ is defined as a standard Hill function given by

$$f(C_M) = \frac{\beta C_M^n}{k^n + C_M^n}. \tag{3.21}$$

Multiple sources

To simulate the diffusion of MMPs from multiple sources, we look at the work developed by Travasso *et al.* [117, 118] on binary and ternary phase separation of polymeric mixtures. While this work describes the process of phase separation in an immiscible ternary A/B/C mixture, where all components separate simultaneously with a reversible chemical reaction between A and B (with forward and reverse reaction rate coefficients Γ^+ and Γ^-), we are only interested in the equations that describe the separation in a binary blend. This model is characterized by the order parameter ρ, and has solutions that resemble small circular domains in an hexagonal lattice that will be used to model MMP sources in the tumour. The reaction between the two constituents A and B is,

$$A \underset{\Gamma^-}{\overset{\Gamma^+}{\rightleftarrows}} B, \tag{3.22}$$

and the spatiotemporal dynamics of the two constituents is as follows

$$\frac{\partial \rho}{\partial t} = M_\rho \nabla^2 \omega_\rho - \left(\Gamma^+ + \Gamma^-\right)\rho + \left(\Gamma^- - \Gamma^+\right). \tag{3.23}$$

Eq. (3.23) describes a lamellar phase, when $\Gamma^+ = \Gamma^-$, and an hexagonal lattice of small circular domains when $\Gamma^+ \gg \Gamma^-$ or when $\Gamma^+ \ll \Gamma^-$, which is what is pretended. Setting $r = \frac{\Gamma^-}{\Gamma^+}$ and $\Gamma_0 = \Gamma^+ + \Gamma^-$ we get

$$\frac{\partial \rho}{\partial t} = M_\rho \nabla^2 \omega_\rho - \Gamma_0 \rho + \Gamma_0 \left(\frac{r-1}{r+1}\right), \tag{3.24}$$

where M_ρ is the mobility of the order parameter ρ. The chemical potential, ω_ρ, is given by,

$$\omega_\rho = \frac{\delta F(\rho)}{\delta \rho}, \tag{3.25}$$

where the free energy functional, F(ρ), is given by,

$$F(\rho) = \int d\mathbf{r} \left[f(\rho) + \frac{1}{2}(\nabla \rho)^2 \right]. \tag{3.26}$$

Finally, the local free energy, $f(\rho)$, takes the form

$$f(\rho) = -\frac{\rho^2}{2} + \frac{\rho^4}{4}, \tag{3.27}$$

from which we get

$$\omega_\rho = \frac{\delta F(\rho)}{\delta \rho} \implies \omega_\rho = f'(\rho) - (\nabla^2 \rho). \tag{3.28}$$

Lastly, to facilitate the creation of MMP domains we add a new fluctuating term to Eq. (3.24). Let X represent a random variable uniformly distributed in the interval [0, 1],

$$\frac{\partial \rho}{\partial t} = M_\rho \nabla^2 \omega - \Gamma_0 \rho + \Gamma_0 \left(\frac{r-1}{r+1} \right) + (X - 0.5) \frac{10}{\cosh^2 \left(\frac{(\rho + 0.5)}{0.2} \right)}. \tag{3.29}$$

Eq. (3.24) will be used to simulate MMP production sites inside the tumour. With this aim, Γ_0 will be set to a low value inside the tumour and to a large value outside (Figure 3.2).

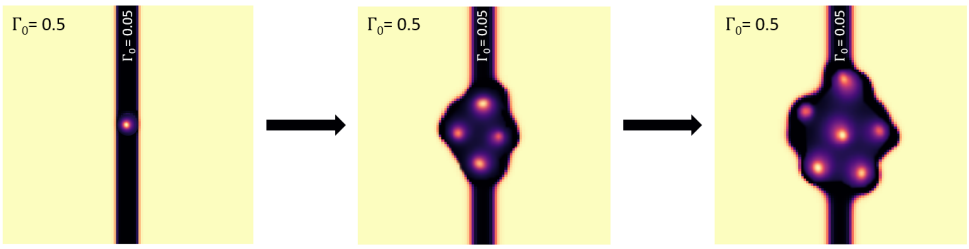

Figure 3.2: **Representation of the evolution of the hexagonal lattice of small circular domains**, effectively degrading the ECM of the duct (in black) and invading the stroma (in yellow).

We can manipulate this hexagonal pattern-producing system to simulate the appearance and consequent diffusion of MMPs, that will then degrade the ECM of the duct. This is done by altering equation (3.19), in by modulating the production term, α, in a way that makes this production dependent on the order parameter ρ, like so,

$$\frac{\partial C_M}{\partial t} = D_{C_M} \nabla^2 C_M + \alpha g(\rho) - \zeta C_M, \tag{3.30}$$

with

$$g(\rho) = 0.5 \left(\tanh \left(\frac{\rho - 0.7}{0.2} \right) + 1 \right). \tag{3.31}$$

At which point we can alter equation (3.20), multiplying the last term by the order parameter ψ, ensuring that the hexagonal pattern (now our sources of MMPs), only develop inside the duct,

$$\frac{\partial \psi}{\partial t} = D_\psi \frac{\tau}{\tau_D} \nabla^2 \psi - \frac{1}{\tau_D} \frac{dF(\psi)}{d\psi} - \eta\mu \frac{\tau}{\tau_D} \frac{dG(\phi, \psi)}{d\psi} + \lambda \frac{\tau}{\tau_D} \hat{c} |\nabla \psi| - f(C_M)\psi. \tag{3.32}$$

Chapter 4
Results & Discussion

In the present chapter we present the obtained results, starting by clarifying the initial conditions used in our model (**Section 4.1**). We then explore the mechanisms of proliferation of the tumour (**Section 4.1.1**), how the characteristics of the prostatic ducts influence the morphology of the structure (**Section 4.1.2**), and finally we discuss how the curve-dependent term affects the system (**Section 4.1.3**). Lastly, we provide and analyze the results of introducing a singular (**Section 4.1.4**), and multiple (**Section 4.1.5**) sources of MMPs.

4.1 Initial Conditions

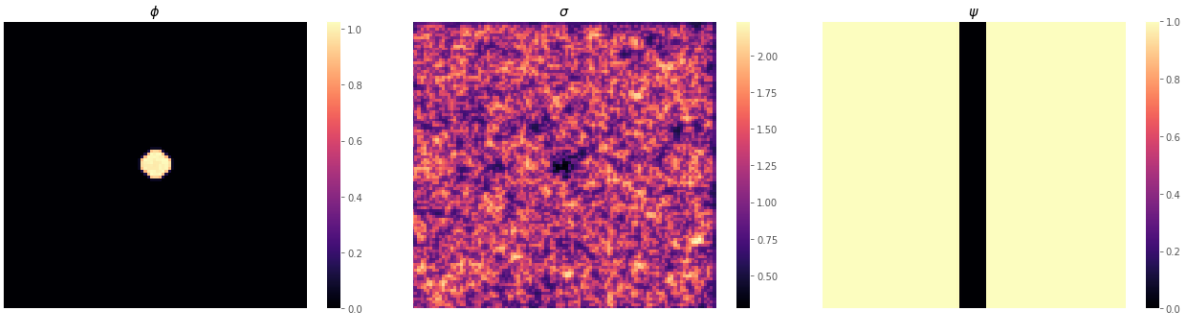

Figure 4.1: **Initial conditions.** Tumour (ϕ), nutrient (σ) and duct (ψ), when t = 1 d.

The simulations were run on a 1510 μm x 1510 μm 2D computational domain, with a spacing between points of 15.1 μm. We assume periodic boundary conditions (PBCs) and the values for the different parameters were taken from the work of Lorenzo *et al.* [6, 119]. In table 4.1 we present the values for the different parameters used in the model.

Initially, the tumour is represented by a circle with a radius of 72.48 μm. The nutrient is heterogeneously distributed in the space, and diffuses from blood vessels represented as squares with 24.4 μm side, with a vascular density of 59.9 [113], i.e. 59.9% of the space is covered by the blood vessels. Eq. (3.11), governs the nutrient distribution inside the blood vessels, while the

rest of the space has a baseline value for the nutrient production of 0.5 g·$L^{-1}d^{-1}$. We consider the prostatic duct to have a diameter of 151 μm [76, 77]. In our 2D simulation, we can see the tumour inside the prostatic duct, in the nutrient-containing tissue (Figure 4.1). This is the basis of the model, given by Eqs. (3.11), (3.14), and (3.16).

Table 4.1: **Parameter values**.

Parameter	**Description**	**Value**
$D_\phi = D_\sigma = D_\psi$	Diffusivity of the phase-field	900 $\mu\text{m}^2 \cdot \text{d}^{-1}$
τ	Interface relaxation time	3.65 d
χ	Nutrient-driven growth	2.8 g $\cdot$ $\text{L}^{-1} \cdot \text{d}^{-1}$
A	Apoptosis rate	1.6438 d^{-1}
s	Nutrient supply	5.5 ± 2.75 g $\cdot$ $\text{L}^{-1} \cdot \text{d}^{-1}$
δ	Nutrient consumption rate	2.75 g $\cdot$ L^{-1}
γ	Nutrient decay rate	2.76 d^{-1}
τ_D	Interface relaxation time*	— d
μ	Duct's resistance to infiltration*	—
η	Tumour vs. duct interface ratio	10
α	MMP production coefficient	1 d^{-1}
ζ	MMP degradation coefficient	0.2 d^{-1}
k	MMP concentration where $f(C_M) = 0.5$	0.2
n	Hill coefficient	15
β	ECM degradation rate	85
Γ_0	$\Gamma^+ + \Gamma^-$	0.5
r	$\frac{\Gamma^-}{\Gamma^+}$	3

*varying values

4.2 Proliferation of the tumour

Tumour growth will depend on the cell's proliferation rate, the apoptosis rate coefficient, and on their nutrient availability. With a fixed nutrient distribution and apoptosis rate for the cells, we can see how the tumour proliferation rate affects the tumour's ability to survive.

Logically, the higher the value of the proliferation rate the faster the tumour grows and spreads. While the initial shape for the tumour is a circle, as it grows we see the edges of the

tumour become more rugged. This is due to the heterogeneity of the nutrient supply which drives growth along the gradients of σ resulting in this shape instability. This effect can be visualized in Figure 4.2, and even more clearly in Figure 4.3, which shows the percentage of area occupied by the tumour for different values of χ over time. We observe that there is a minimum threshold which allows for tumour growth (approximately $\chi = 2.4$ for the parameters used), otherwise the tumour shrinks. With this, we will set $\chi = 2.8$ for the following simulations, allowing for a steady growth of the tumour mass.

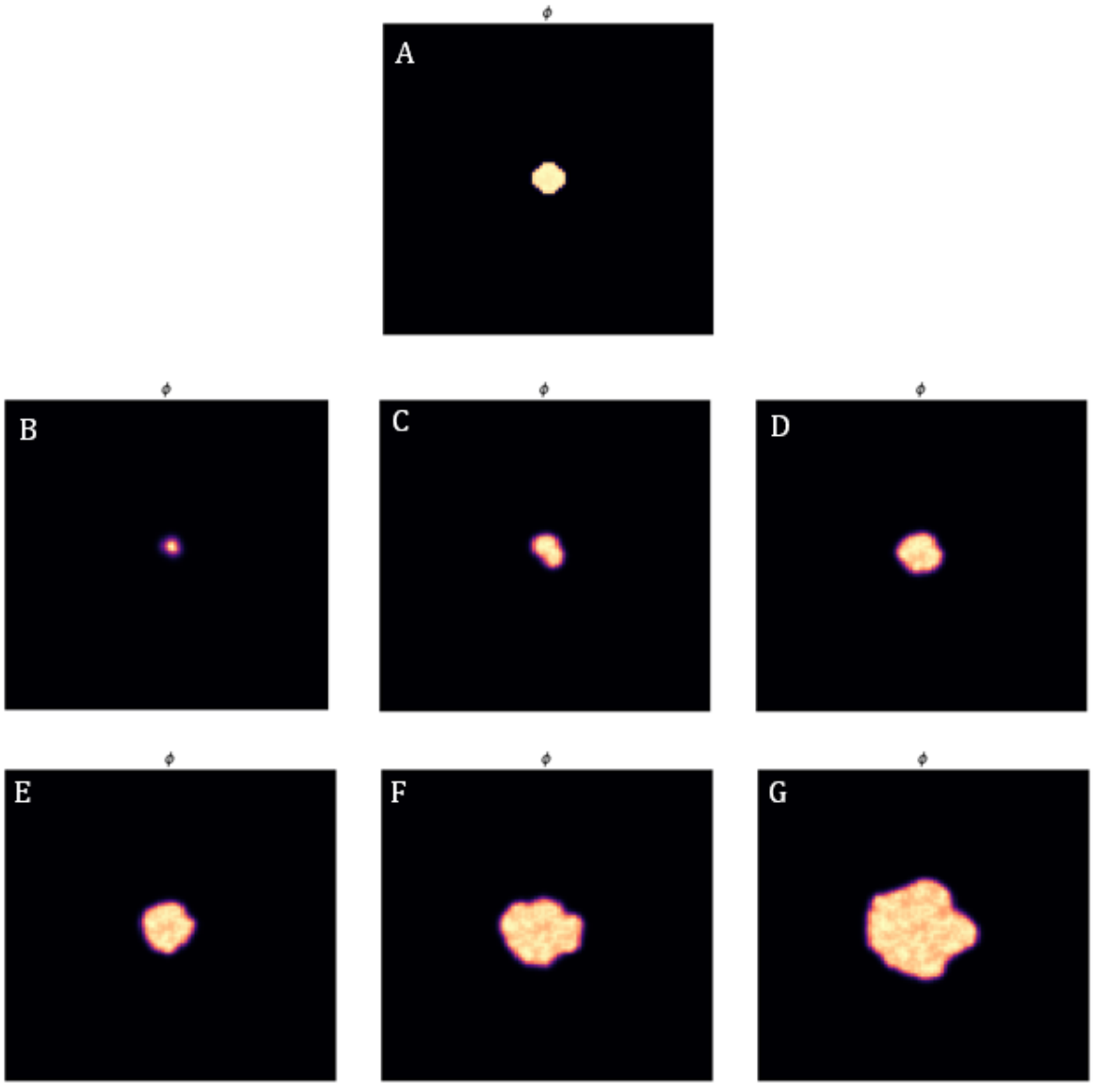

Figure 4.2: **Tumour growth for each χ value tested.** A corresponds to the initial condition, with B, C, D, E , F and G, corresponding to the state of the tumour at t = 500 d for different values of χ (2.2, 2.3, 2.4, 2.5, 2.8, 3.1, respectively).

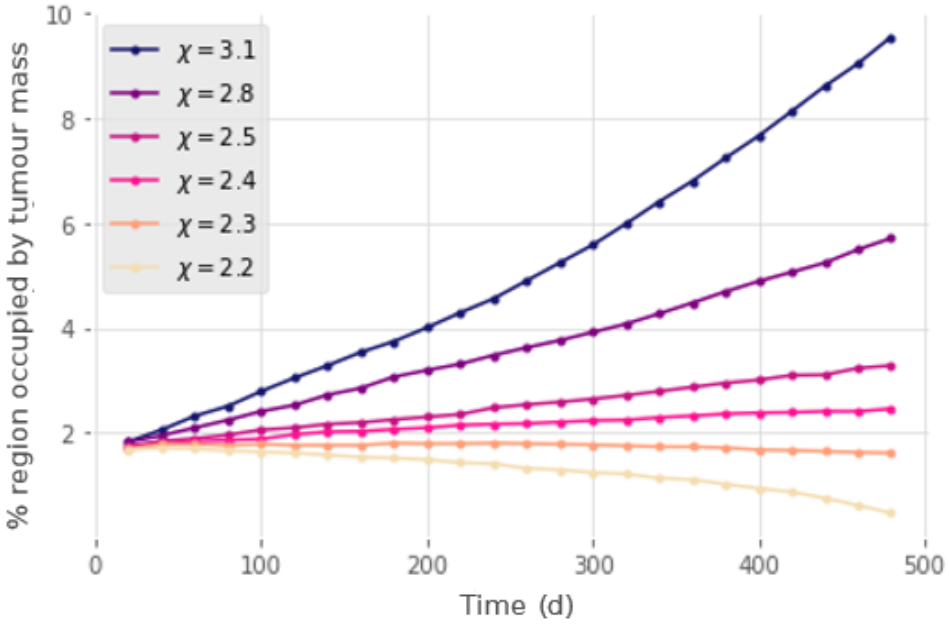

Figure 4.3: **Percentage of the simulated region occupied by the tumour mass for different values of χ, over time.**

4.3 Tumour growth affects duct morphology

As discussed before, the morphology of the ductal structure is affected by the process of tumourigenesis, and vice-versa, through a plethora of biochemical processes which are yet to be understood in their entirety. When tumour growth initiates inside a prostatic duct the morphology of the tissue gradually changes from healthy prostatic acini with empty lumens, giving rise to PIN (characterised by luminal cell hyperplasia), and eventually leading to invasive carcinoma, giving rise to the different GPs (consequence of tumour-promoting changes in the microenvironment).

The proliferation of the tumour will thus either naturally deform the ductal structure, or it will cause the lumens to be entirely invaded by the tumour without being significantly deformed.

This process was simulated by Eqs. 3.11, 3.14, and 3.17, and by varying the two parameters responsible for the tumour-duct interaction, τ_D and μ. As clarified before, the value of μ regulates the permeability of the tumour in the tissue, while the value of τ_D describes the mobility of the duct's walls. (Table 4.2).

With this, Figures 4.4 and 4.5 show the evolution of tumour growth inside a duct for different values of τ_D (10, 30, and 50), and for values of μ of 2 and 0.2. For the higher value of $\mu = 2$ resistance to infiltration is substantial, which means that the tumour cannot freely leave the duct, and follows the direction of the duct (Figure 4.4). When we lower this value, we see that

Table 4.2: **Effects of μ and τ_D on the duct dynamics.**

	Low	High
μ	Tumour less restricted to duct	Tumour more restricted to duct
τ_D	Flexible duct	Rigid duct

the tumour is less restricted to the duct, and thus is able to grow outside the duct's domain (Figure 4.5, bottom row). This effect is exacerbated as we increase the value of τ_D i.e., as we increase the rigidity of the duct (comparing the bottom right and bottom left images of Figure 4.5, for example).

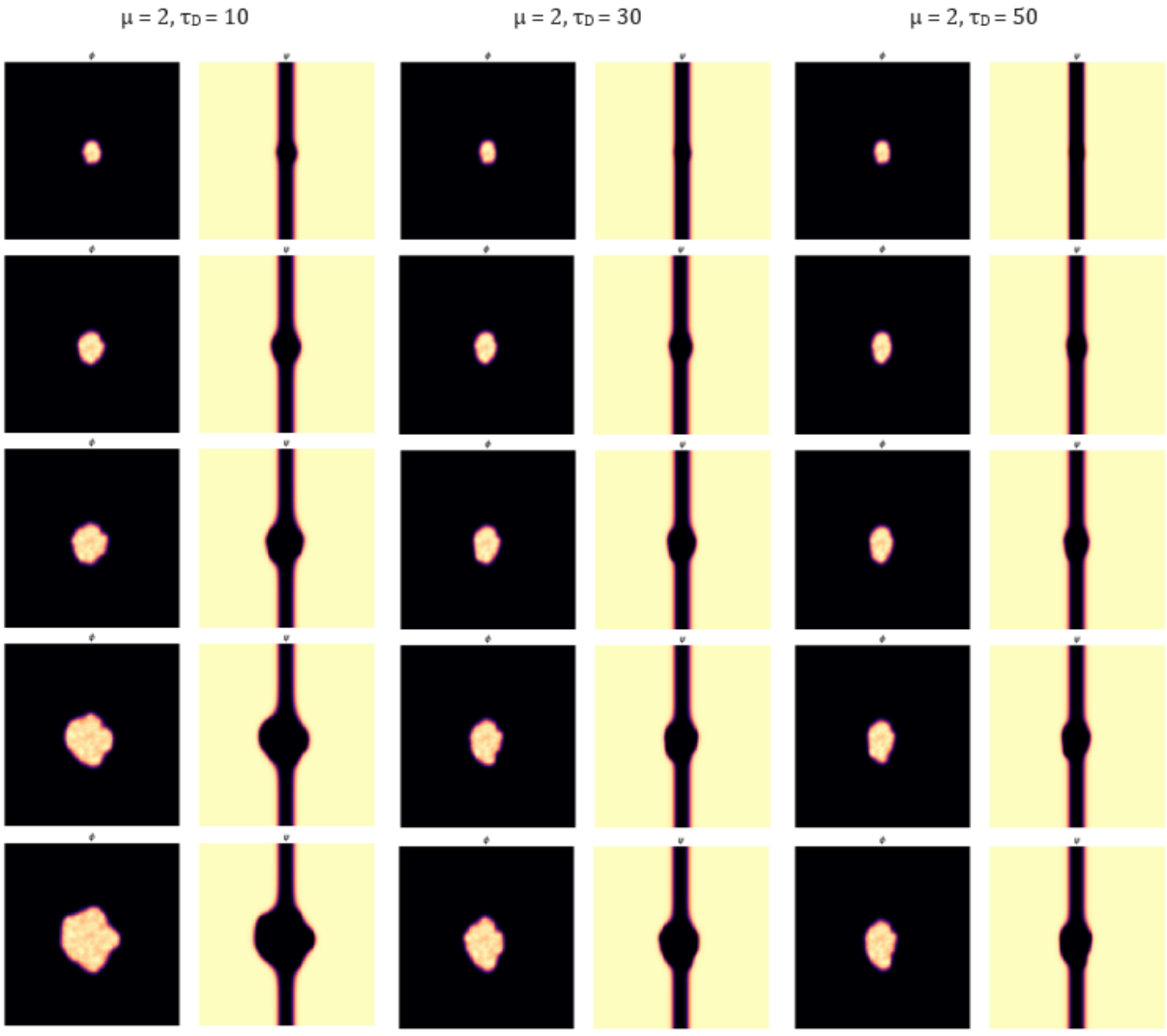

Figure 4.4: **Growth of a tumour restricted to the interior of a duct and its deformation for different values of τ_D, and a fixed value of μ.** From top to bottom row, t = 1, t = 100 d, t = 400 d, t = 700 d, t = 1000 d

On the other hand, the decrease of the mobility of the duct's walls influences the morphology of the tumour for $\mu = 2$, with the tumour growing within the path imposed by the duct, and not leaving it. As τ_D increases, the tumour is gradually more constricted and unable to meaningfully distort the duct (Figure 4.4, left column).

Comparing tumour morphology for both cases it is clear that the higher freedom of movement related to lower μ and τ_D facilitates the invasion of the stroma, as the duct is malleable and less energy is required for the tumour to leave the imposed path. The complete restriction of the tumour to the duct can only be achieved when setting both these parameters to higher values.

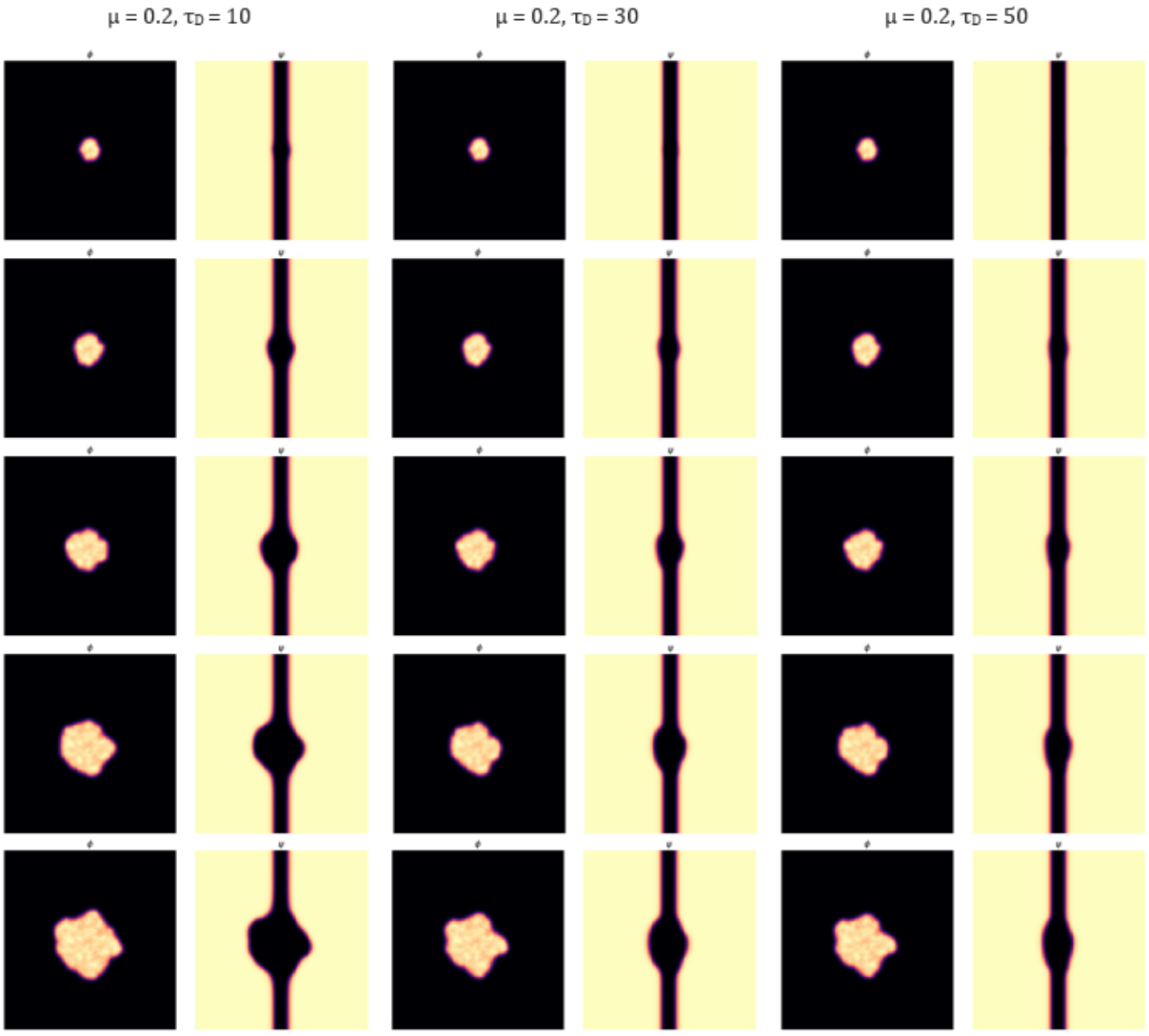

Figure 4.5: **Growth of a tumour restricted to the interior of a duct and its deformation for different values of τ_D, and a fixed value of μ.** From top to bottom row, t = 1, t = 100 d, t = 400 d, t = 700 d, t = 1000 d

4.4 Implications of the curvature-dependent term

The curvature-dependent term added to the model by Paiva [115], first proposed by Biben *et al.* [116] cancels the surface tension between the duct and the tissue. This term will be important to permit the development of new ducts.

To address how necessary the addition of this term was we sought to determine how significant was the influence of surface tension. To this effect, we simulated a circular domain of tissue to study its evolution under the influence of surface tension (Figure 4.6).

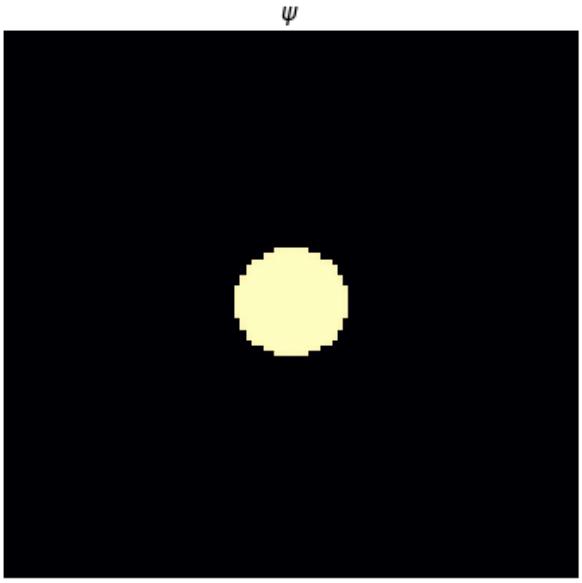

Figure 4.6: **Circular tissue domain**

The phase-field for the order parameter ψ was then calculated over time, for two cases:

- With the curve-dependent term:

$$\frac{\partial \psi}{\partial t} = D_\psi \frac{\tau}{\tau_D} \nabla^2 \psi - \frac{1}{\tau_D} \frac{dF(\psi)}{d\psi} - \eta\mu \frac{\tau}{\tau_D} \frac{dG(\phi, \psi)}{d\psi} + D_\psi \frac{\tau}{\tau_D} \hat{c} |\nabla \psi|$$

- Without the curve-dependent term:

$$\frac{\partial \psi}{\partial t} = D_\psi \frac{\tau}{\tau_D} \nabla^2 \psi - \frac{1}{\tau_D} \frac{dF(\psi)}{d\psi} - \eta\mu \frac{\tau}{\tau_D} \frac{dG(\phi, \psi)}{d\psi}$$

What is expected is that this term acts a stabilizing force on the interface by counteracting the surface tension introduced by the duct's wall that works towards minimizing the area of the interface, while maintaining an hyperbolic tangent profile (which implies that the interface between the phases changes smoothly and gradually as it moves). Therefore, without the curvature-dependent term, the circular shape would decrease in size over time, as the system minimizes the interface area.

Looking at the percentage of the area occupied by the tissue over time (Figure 4.7), it is clear that the curvature-dependent term does in fact contribute to stop a decrease of the circle's area, when compared to the results of the simulation without this term.

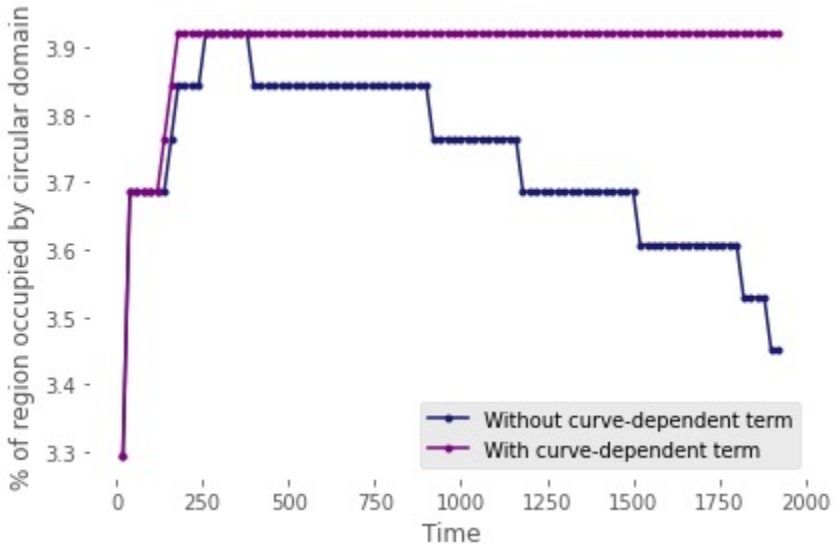

Figure 4.7: **Percentage of the simulated region occupied by the circle, over time.**

4.5 Singular source of MMPs

In this section, we present the results of our simulation with a focus on the influence of a singular source of MMPs for ECM degradation, and investigate how the presence of an MMP source affects tumour progression, duct deformation, and branching behavior.

The system is now simulated by Eqs. (3.11), (3.14), and (3.20). We introduce a new equation (Eq. (3.19)) which models the dynamics of MMP concentration, including a production coefficient $\alpha(\vec{r})$, which represents the MMP source and a degradation coefficient, ζ.

The degradation of the ECM of the duct itself is achieved by the last term in Eq. (3.20), which modulates the degree of degradation based on the MMP concentration using a Hill function. The MMPs diffuse from a circular region located specifically at the interface of the duct, and follow the movement of the interface as the system evolves and the tumour grows and deforms the duct. As the MMPs diffuse into the ECM, they degrade it, allowing the tumour to invade the tissue and causing the duct to deform.

The simulation results demonstrate that the introduction of the singular source for ECM degradation successfully impacts the system's behavior. In Figures 4.8 and 4.9, we show the results of the simulation, where the MMPs are produced and diffused from the circular source,

creating regions of ECM degradation. The tumour takes advantage of these regions, invading the degraded ECM and spreading further into the stroma. The ECM degradation leads to a restructuring of the ducts' architecture, causing them to deform under the influence of tumour growth.

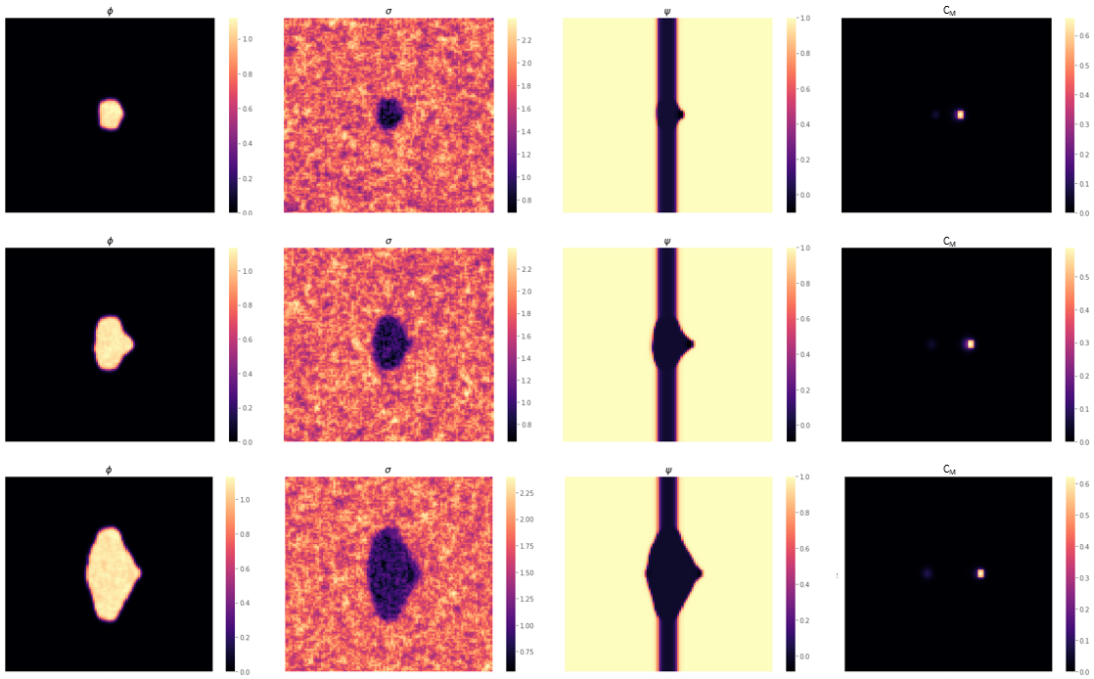

Figure 4.8: **Growth of a tumour mass (ϕ) restricted to the interior of a duct (ψ) whose ECM is being degraded by the action of MMPs (C_M) for high MMP degradation.** From left to right: tumour (ϕ), nutrient (σ), duct (ψ), and MMP concentration (C_M) evolution.

The production and degradation coefficients ($\alpha(\vec{r})$ and ζ) dictate the evolution of the C_M, and need to be appropriately balanced to maintain steady values, otherwise the source of MMPs will be more diffuse in nature (Figure 4.10), leading to a degradation of the duct that is less focused, such as the one reproduced in Figures 4.8 and 4.9.

While the production and degradation coefficients dictate the evolution of the C_M, it is the last term in Eq. (3.20) that dictates how the ECM of the duct is degraded, namely parameters n and k of the Hill function, which were chosen based on the values of the concentration of MMPs, as well as the ECM degradation rate β.

Parameters τ_D and μ also affect how fast the formation of the new branch happens, as seen in Figures 4.8 and 4.9 since the malleability of the duct and the ease with which the tumour can escape it influence the path taken by the tumour as it grows. If the tumour is more restricted to the inside (Figure 4.8), as the ECM gets degraded the tumour will grow into this new path of

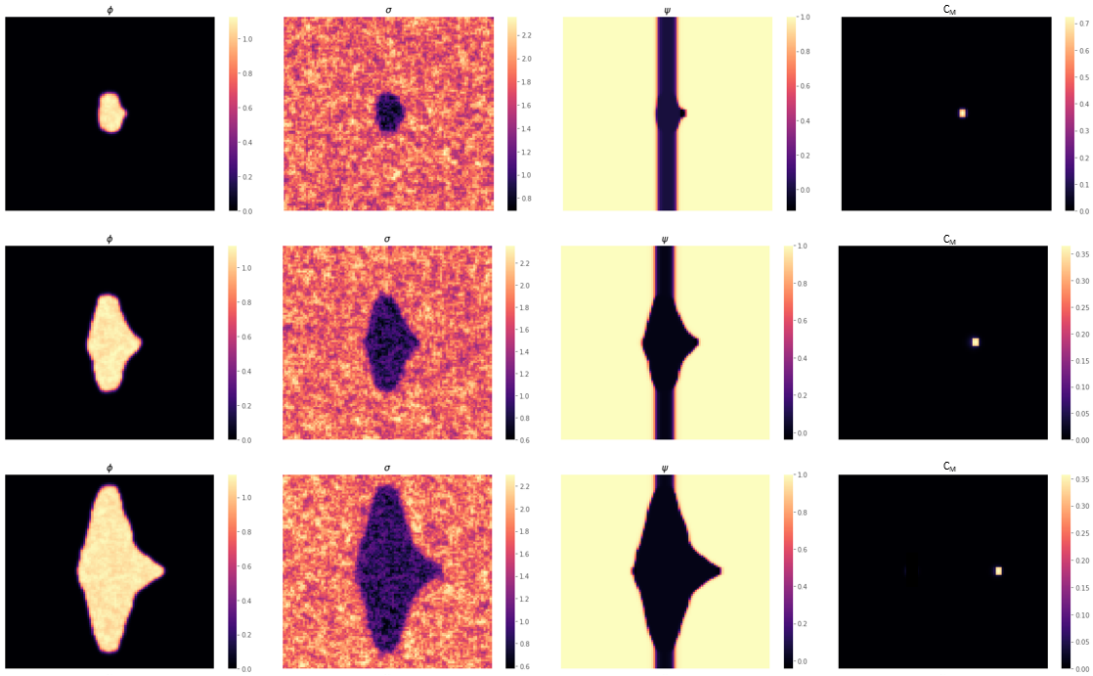

Figure 4.9: **Growth of a tumour mass (ϕ) restricted to the interior of a duct (ψ) whose ECM is being degraded by the action of MMPs (C_M) for high MMP degradation.** From left to right: tumour (ϕ), nutrient (σ), duct (ψ), and MMP concentration (C_M) evolution.

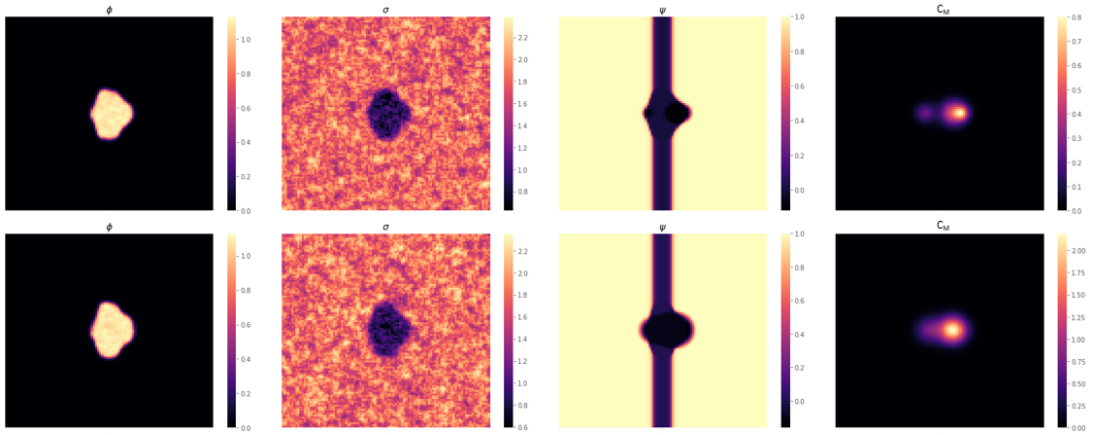

Figure 4.10: **Growth of a tumour mass (ϕ) restricted to the interior of a duct (ψ) whose ECM is being degraded by the action of MMPs (C_M), for low MMP degradation.** From left to right: tumour (ϕ), nutrient (σ), duct (ψ), and MMP concentration (C_M) evolution.

less resistance more easily, as opposed to a more malleable duct (Figure 4.9), where the tumour can more easily grow and deform the duct.

Overall, Eq. (3.20) is an interesting way to modulate ECM degradation, being able to reproduce mechanisms driving tumour invasion, duct deformation, and branching behaviour that take place in tumourigenesis, altering the normal architectural structure of the tissue. It also allows parameter tweaking that could potentially simulate different GP formation as observed in clinical samples.

4.6 Multiples source of MMPs

In this section, we explore the system's evolution when considering the diffusion of MMPs from multiple sources, represented by the hexagonal lattice of small circular domains. These sources act as catalysts for the degradation of the ECM in the ducts, leading to duct deformation and the formation of multiple branches. We contrast this scenario with the previous approach of using a singular MMP source.

The results presented in this section were simulated by Eqs. 3.11, 3.14 and 3.32 which describe the dynamics of the duct's deformation and branching under the influence of MMP diffusion and degradation. The dynamics of MMP concentration are now governed by Eq. (3.30), with the production coefficient being modulated by Eq. (3.31), which in turn is dependent on the order parameter ρ (Eq. (3.29)), responsible for the appearance of small circular domains in an hexagonal lattice (our circular sources of MMPs).

In the same way as the previous case, the production and degradation coefficients influence the evolution of the C_M, and it is the last term in Eq. (3.32) that determines how the ECM of the duct is degraded.

Unlike the single source scenario, the sources of MMP, multiply over time inside the tumour and act at the interface of the duct. Parameter Γ_0 played a crucial role in determining the appearance of the hexagonal lattice of small circular domains inside the tumour, since it depends on the value of ϕ. When $\phi = 1$, Γ_0 was selected such that the hexagonal pattern emerged, and the subsequent MMP diffusion within the ducts initiated the degradation process .

Figures 4.11, and 4.12, show the evolution of the system over time, where MMP action breakdowns the ECM allowing the tumour to deform the duct and invade the stroma, allowing the formation of not only one, but multiple branches over time.

Tumour progression and duct deformation is influenced by various parameters, such as duct mobility, the duct's resistance to infiltration, MMP production, and degradation.

Once again, the mobility of the ducts influenced the overall deformation pattern and branching behaviour, with a lower value of τ_D allowing for more substantial deformation and branching (Figure 4.12) when compared to a higher value (Figure 4.11).

In our simulations, we observed that the presence of multiple MMP sources significantly influenced the system's behavior compared to a single source scenario. The simultaneous degradation of the ECM from various points within the duct led to more complex and irregular patterns of branching, resulting in a greater tumor invasion into the surrounding stroma.

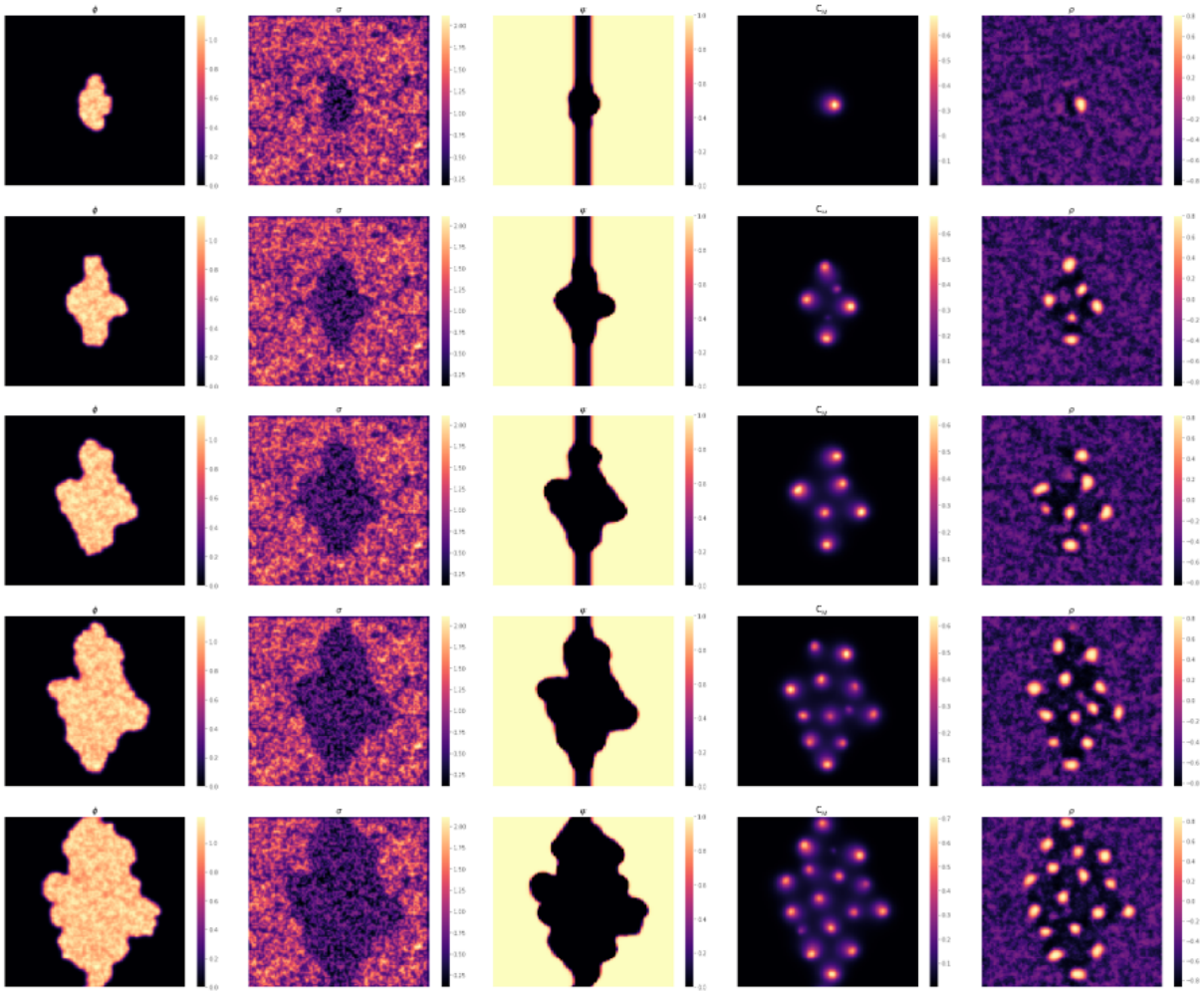

Figure 4.11: **Growth of a tumour mass (ϕ) restricted to the interior of a duct (ψ) whose ECM is being degraded by the action of MMPs (C_M).** From left to right: tumour (ϕ), nutrient (σ), duct (ψ), MMP concentration (C_M), and order parameter ρ evolution.

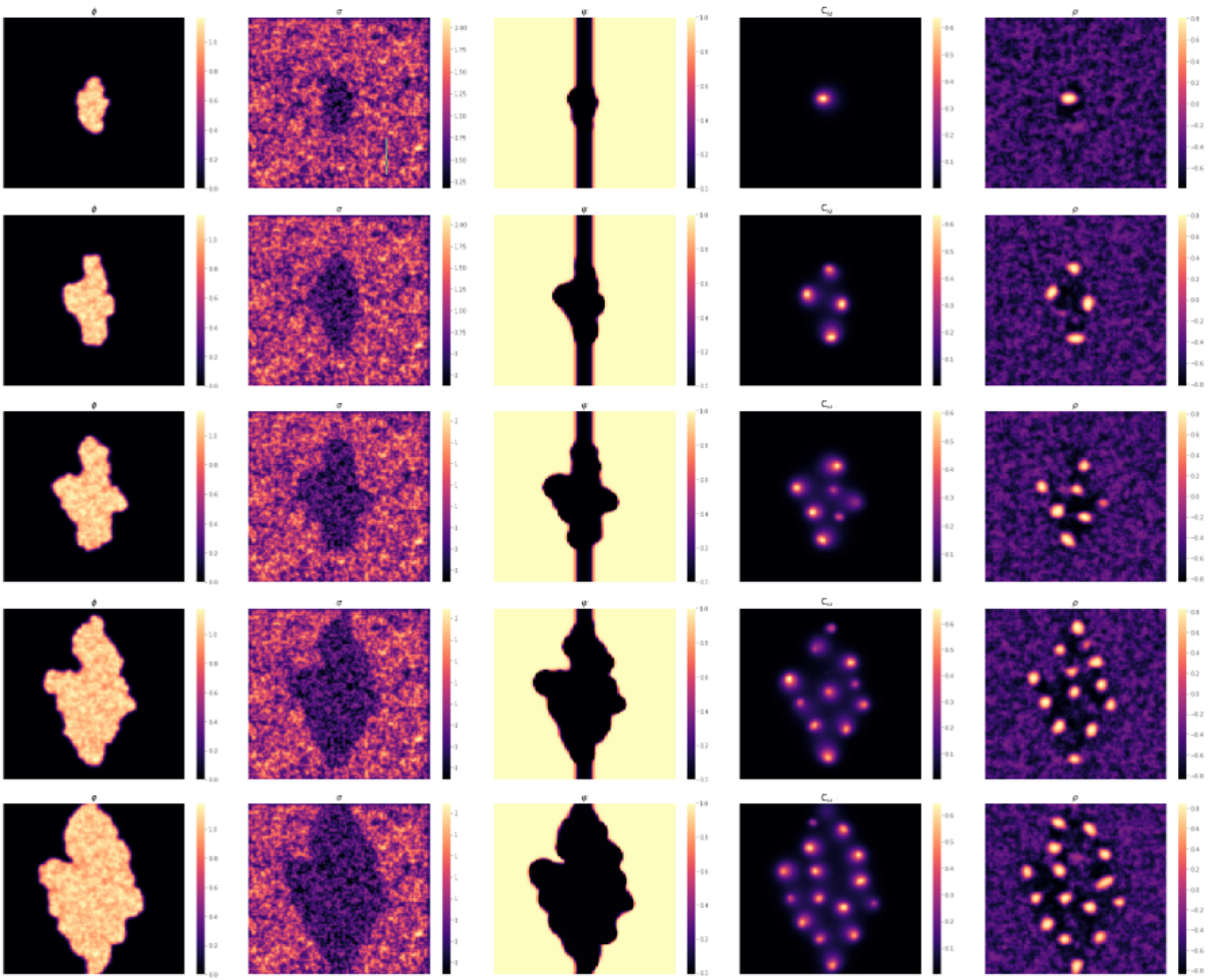

Figure 4.12: **Growth of a tumour mass (ϕ) restricted to the interior of a duct (ψ) whose ECM is being degraded by the action of MMPs (C_M).** From left to right: tumour (ϕ), nutrient (σ), duct (ψ), MMP concentration (C_M), and order parameter ρ evolution.

Chapter 5

Conclusion

The 2D phase-field model described in this work is an extension of the work from Lorenzo *et al.* [6]. A set of reaction-diffusion equations are used in the proposed model to describe the dynamics of important components driving the development of the disease (such as nutrient and MMPs), and the phase-field method is used to depict the tumour and the prostatic ducts. With a focus on tumour branching and the deterioration of the ECM that makes up the ductal structure, we examined how alterations in the model parameters affect PCa dynamics.

While there are improvements to be made to the model developed, it was possible to simulate the evolution of tumourigenesis in PCa, and how parameters such as the proliferation rate affected the growth of the tumour. We also explored how the parameters that governed the duct dynamics (namely the duct's resistance to infiltration, μ, and the interface relaxation time, τ_D) affected the morphology of the tissue, specifically the interaction between duct and tumour. Additionally, we sought to understand how and if the curvature-dependent term used to calculate the order parameter ψ significantly altered the system's evolution.

We presented new equations that model the dynamics of MMPs (a singular source and multiple sources), responsible for degrading the ECM of the duct. The results of our simulations show potential for this approach at reproducing the branching process and GP formation, revealing the complexity of tumour growth and its interaction with the underlying ductal structure.

The singular source equation for ECM degradation permitted to modulate the formation of a single branch, thus altering the architecture of the system. The MMP source introduced a localized ECM degradation, providing a pathway for the tumour to invade the healthy tissue.

The ability to model multiple sources of MMP that act to degrade the duct's ECM could be a valuable tool for studying tumour behaviour under more realistic conditions, and by adjusting the parameters, we can further reproduce the impact of specific factors on tumour invasion and branching, as well as the formation of different GPs.

The formation of new ducts was achieved by introducing **localized** MMP production, specifically by adding circular sources that acted at the interface of the duct. On the other hand, a

generalized MMP production by all the tumor cells resulted in a faster invasion of the tumour since ultimately all of the ECM was being degraded, and the tumour grew into a rounded shape inside the duct, without forming new ducts or adopting an irregular morphology. This indicates that there must be cell specialization in tumour behaviour, namely cell specialization responsible for MMP dynamics and ECM degradation, to expand the duct network, as observed in several prostate adenocarcinoma GP5 phenotypes.

Moreover, we propose that the Notch signalling pathway may play a significant role in the development of these GPs in PCa. The relevance of Notch signaling in other tumours, and in particular in the process of angiogenesis, supports the idea that it may also influence the creation of additional ducts in PCa. Further investigations into the Notch pathway's potential impact on tumour morphology and GPs could offer valuable insights into PCa progression.

5.1 Future work

The 2D phase-field model presented lays the foundation for further improvements and exploration. While the current model provided valuable insights into tumour branching and ECM degradation within the prostatic ducts, there are several avenues for future research and enhancements to be pursued.

Firstly, refining the model's parameters would be an improvement to the model, in order for the results to better align with clinical observation. Secondly, to better represent the complexity of the prostatic ductal system, future work can focus on extending the model to include a network of ducts. This enhancement would enable a more realistic depiction of the tumour's interaction with the intricate ductal structure and its impact on branching and tumour growth.

A step further would be to transition from a 2D model to a 3D one, since it would offer a more comprehensive visualization of tumour growth and GP formation in a closer representation of actual physiological conditions.

Bibliography

[1] H. Sung, J. Ferlay, R. L. Siegel, M. Laversanne, I. Soerjomataram, A. Jemal, and F. Bray, "Global cancer statistics 2020: Globocan estimates of incidence and mortality worldwide for 36 cancers in 185 countries," *CA: a cancer journal for clinicians*, vol. 71, no. 3, pp. 209–249, 2021.

[2] R. L. Siegel, K. D. Miller, N. S. Wagle, and A. Jemal, "Cancer statistics, 2023," *CA: a cancer journal for clinicians*, vol. 73, no. 1, pp. 17–48, 2023.

[3] H. Van Poppel, T. Albreht, P. Basu, R. Hogenhout, S. Collen, and M. Roobol, "Serum psa-based early detection of prostate cancer in europe and globally: Past, present and future," *Nature Reviews Urology*, vol. 19, no. 9, pp. 562–572, 2022.

[4] H. Schatten, "Cell & molecular biology of prostate cancer," *Advances in Experimental Medicine and Biology*, vol. 1095, pp. 1–14, 2018.

[5] S. Loeb, M. A. Bjurlin, J. Nicholson, T. L. Tammela, D. F. Penson, H. B. Carter, P. Carroll, and R. Etzioni, "Overdiagnosis and overtreatment of prostate cancer," *European urology*, vol. 65, no. 6, pp. 1046–1055, 2014.

[6] G. Lorenzo, M. A. Scott, K. Tew, T. J. Hughes, Y. J. Zhang, L. Liu, G. Vilanova, and H. Gomez, "Tissue-scale, personalized modeling and simulation of prostate cancer growth," *Proceedings of the National Academy of Sciences*, vol. 113, no. 48, pp. E7663–E7671, 2016.

[7] T. Phan, S. M. Crook, A. H. Bryce, C. C. Maley, E. J. Kostelich, and Y. Kuang, "Mathematical modeling of prostate cancer and clinical application," *Applied Sciences*, vol. 10, no. 8, p. 2721, 2020.

[8] E. Yorke, Z. Fuks, L. Norton, W. Whitmore, and C. Ling, "Modeling the development of metastases from primary and locally recurrent tumors: comparison with a clinical data base for prostatic cancer," *Cancer research*, vol. 53, no. 13, pp. 2987–2993, 1993.

[9] T. L. Jackson, "A mathematical model of prostate tumor growth and androgen-independent relapse," *Discrete and Continuous Dynamical Systems-B*, vol. 4, no. 1, pp. 187–201, 2003.

[10] A. M. Ideta, G. Tanaka, T. Takeuchi, and K. Aihara, "A mathematical model of intermittent androgen suppression for prostate cancer," *Journal of nonlinear science*, vol. 18, pp. 593–614, 2008.

[11] T. Shimada and K. Aihara, "A nonlinear model with competition between prostate tumor cells and its application to intermittent androgen suppression therapy of prostate cancer," *Mathematical biosciences*, vol. 214, no. 1-2, pp. 134–139, 2008.

[12] Q. Guo, Y. Tao, and K. Aihara, "Mathematical modeling of prostate tumor growth under intermittent androgen suppression with partial differential equations," *international Journal of Bifurcation and Chaos*, vol. 18, no. 12, pp. 3789–3797, 2008.

[13] Y. Tao, Q. Guo, and K. Aihara, "A mathematical model of prostate tumor growth under hormone therapy with mutation inhibitor," *Journal of nonlinear science*, vol. 20, pp. 219–240, 2010.

[14] J. Yang, T.-J. Zhao, C.-Q. Yuan, J.-H. Xie, and F.-F. Hao, "A nonlinear competitive model of the prostate tumor growth under intermittent androgen suppression," *Journal of theoretical biology*, vol. 404, pp. 66–72, 2016.

[15] H. A. Barton and M. E. Andersen, "A model for pharmacokinetics and physiological feedback among hormones of the testicular-pituitary axis in adult male rats: a framework for evaluating effects of endocrine active compounds," *Toxicological Sciences*, vol. 45, no. 2, pp. 174–187, 1998.

[16] L. K. Potter, M. G. Zager, and H. A. Barton, "Mathematical model for the androgenic regulation of the prostate in intact and castrated adult male rats," *American Journal of Physiology-Endocrinology and Metabolism*, vol. 291, no. 5, pp. E952–E964, 2006.

[17] T. Reckell, K. Nguyen, T. Phan, S. Crook, E. J. Kostelich, and Y. Kuang, "Modeling the synergistic properties of drugs in hormonal treatment for prostate cancer," *Journal of theoretical biology*, vol. 514, p. 110570, 2021.

[18] M. Cerasuolo, F. Maccarinelli, D. Coltrini, A. M. Mahmoud, V. Marolda, G. C. Ghedini, S. Rezzola, A. Giacomini, L. Triggiani, M. Kostrzewa, *et al.*, "Modeling acquired resistance

to the second-generation androgen receptor antagonist enzalutamide in the tramp model of prostate cancer," *Cancer Research*, vol. 80, no. 7, pp. 1564–1577, 2020.

[19] H. V. Jain, S. K. Clinton, A. Bhinder, and A. Friedman, "Mathematical modeling of prostate cancer progression in response to androgen ablation therapy," *Proceedings of the National Academy of Sciences*, vol. 108, no. 49, pp. 19701–19706, 2011.

[20] H. V. Jain and A. Friedman, "Modeling prostate cancer response to continuous versus intermittent androgen ablation therapy," *Discrete and Continuous Dynamical Systems-B*, vol. 18, no. 4, pp. 945–967, 2013.

[21] J. B. West, M. N. Dinh, J. S. Brown, J. Zhang, A. R. Anderson, and R. A. Gatenby, "Multidrug cancer therapy in metastatic castrate-resistant prostate cancer: An evolution-based strategyevolutionary dynamics in multidrug therapy," *Clinical Cancer Research*, vol. 25, no. 14, pp. 4413–4421, 2019.

[22] H. Peng, W. Zhao, H. Tan, Z. Ji, J. Li, K. Li, and X. Zhou, "Prediction of treatment efficacy for prostate cancer using a mathematical model," *Scientific reports*, vol. 6, no. 1, p. 21599, 2016.

[23] E. M. Rutter and Y. Kuang, "Global dynamics of a model of joint hormone treatment with dendritic cell vaccine for prostate cancer," *Discrete & Continuous Dynamical Systems-B*, vol. 22, no. 3, p. 1001, 2017.

[24] M. Elishmereni, Y. Kheifetz, I. Shukrun, G. H. Bevan, D. Nandy, K. M. McKenzie, M. Kohli, and Z. Agur, "Predicting time to castration resistance in hormone sensitive prostate cancer by a personalization algorithm based on a mechanistic model integrating patient data," *The Prostate*, vol. 76, no. 1, pp. 48–57, 2016.

[25] Y. Hirata, N. Bruchovsky, and K. Aihara, "Development of a mathematical model that predicts the outcome of hormone therapy for prostate cancer," *Journal of theoretical biology*, vol. 264, no. 2, pp. 517–527, 2010.

[26] T. Portz, Y. Kuang, and J. D. Nagy, "A clinical data validated mathematical model of prostate cancer growth under intermittent androgen suppression therapy," *Aip Advances*, vol. 2, no. 1, p. 011002, 2012.

[27] J. Baez and Y. Kuang, "Mathematical models of androgen resistance in prostate cancer patients under intermittent androgen suppression therapy," *Applied Sciences*, vol. 6, no. 11, p. 352, 2016.

[28] T. Phan, C. He, A. Martinez, and Y. Kuang, "Dynamics and implications of models for intermittent androgen suppression therapy," *Mathematical Biosciences and Engineering*, vol. 16, no. 1, pp. 187–204, 2019.

[29] R. T. Vollmer, S. Egawa, S. Kuwao, and S. Baba, "The dynamics of prostate specific antigen during watchful waiting of prostate carcinoma: a study of 94 japanese men," *Cancer*, vol. 94, no. 6, pp. 1692–1698, 2002.

[30] R. T. Vollmer and P. A. Humphrey, "Tumor volume in prostate cancer and serum prostate-specific antigen: analysis from a kinetic viewpoint," *American journal of clinical pathology*, vol. 119, no. 1, pp. 80–89, 2003.

[31] G. Dimonte, "A cell kinetics model for prostate cancer and its application to clinical data and individual patients," *Journal of Theoretical Biology*, vol. 264, no. 2, pp. 420–442, 2010.

[32] G. Dimonte, E. Bergstralh, M. Bolander, R. Karnes, and D. Tindall, "Use of tumor dynamics to clarify the observed variability among biochemical recurrence nomograms for prostate cancer," *The Prostate*, vol. 72, no. 3, pp. 280–290, 2012.

[33] N. Wentzensen, S. Vinokurova, and M. v. K. Doeberitz, "Systematic review of genomic integration sites of human papillomavirus genomes in epithelial dysplasia and invasive cancer of the female lower genital tract," *Cancer research*, vol. 64, no. 11, pp. 3878–3884, 2004.

[34] V. Cristini and J. Lowengrub, *Multiscale modeling of cancer: an integrated experimental and mathematical modeling approach*. Cambridge University Press, 2010.

[35] D. Hanahan and R. A. Weinberg, "Hallmarks of cancer: the next generation," *cell*, vol. 144, no. 5, pp. 646–674, 2011.

[36] N. C. I. U. S. National Institutes of Health, "Seer training modules, cancer registration surveillance." `https://training.seer.cancer.gov/disease/categories/classification.html`, 2021. Accessed May 8, 2023.

[37] S. Standring, *Gray's Anatomy: The Anatomical Basis of Clinical Practice*. Gray's Anatomy Series, Elsevier Limited, 2016.

[38] J. E. McNeal, "Anatomy of the prostate: an historical survey of divergent views," *The prostate*, vol. 1, no. 1, pp. 3–13, 1980.

[39] J. E. McNeal, "The zonal anatomy of the prostate," *The prostate*, vol. 2, no. 1, pp. 35–49, 1981.

[40] A. Partin, R. Dmochowski, A. Wein, C. Peters, and L. Kavoussi, *Campbell-Walsh Urology 12th Edition Review*. Elsevier, 2020.

[41] Cancer Research UK, "Diagram showing the position of the prostate and rectum." `https://commons.wikimedia.org/wiki/File:Diagram_showing_the_position_of_the_prostate_and_rectum_CRUK_358.svg`, 2014. Accessed May 5, 2023.

[42] Mikael Häggström, M.D., "Prostate zones diagram." `https://commons.wikimedia.org/wiki/File:Prostate_zones.png`, 2019. Accessed May 5, 2023.

[43] C. Abate-Shen and M. M. Shen, "Molecular genetics of prostate cancer," *Genes & development*, vol. 14, no. 19, pp. 2410–2434, 2000.

[44] M. M. Shen and C. Abate-Shen, "Molecular genetics of prostate cancer: new prospects for old challenges," *Genes & development*, vol. 24, no. 18, pp. 1967–2000, 2010.

[45] W. Coleman and G. Tsongalis, *Molecular Pathology: The Molecular Basis of Human Disease*. Elsevier Science, 2018.

[46] A. Partin, R. Dmochowski, A. Wein, C. Peters, and L. Kavoussi, *Campbell-Walsh Urology 12th Edition Review*. Elsevier, 2020.

[47] M. M. Collins, R. S. Stafford, M. P. O'LEARY, and M. J. Barry, "How common is prostatitis? a national survey of physician visits," *The Journal of urology*, vol. 159, no. 4, pp. 1224–1228, 1998.

[48] F. U. Khan, A. U. Ihsan, H. U. Khan, R. Jana, J. Wazir, P. Khongorzul, M. Waqar, and X. Zhou, "Comprehensive overview of prostatitis," *Biomedicine & Pharmacotherapy*, vol. 94, pp. 1064–1076, 2017.

[49] C. G. Roehrborn, "Benign prostatic hyperplasia: an overview," *Reviews in urology*, vol. 7, no. Suppl 9, p. S3, 2005.

[50] A. Partin, R. Dmochowski, A. Wein, C. Peters, and L. Kavoussi, *Campbell-Walsh Urology 12th Edition Review*. Elsevier, 2020.

[51] P. Rawla, "Epidemiology of prostate cancer," *World journal of oncology*, vol. 10, no. 2, p. 63, 2019.

[52] K. L. Ng, "The etiology of prostate cancer," *Exon Publications*, pp. 17–27, 2021.

[53] J. R. Packer and N. J. Maitland, "The molecular and cellular origin of human prostate cancer," *Biochimica et Biophysica Acta (BBA)-Molecular Cell Research*, vol. 1863, no. 6, pp. 1238–1260, 2016.

[54] Z. A. Wang, R. Toivanen, S. K. Bergren, P. Chambon, and M. M. Shen, "Luminal cells are favored as the cell of origin for prostate cancer," *Cell reports*, vol. 8, no. 5, pp. 1339–1346, 2014.

[55] P. C. Nowell, "The clonal evolution of tumor cell populations: Acquired genetic lability permits stepwise selection of variant sublines and underlies tumor progression.," *Science*, vol. 194, no. 4260, pp. 23–28, 1976.

[56] R. Leao, C. Domingos, A. Figueiredo, R. Hamilton, U. Tabori, and P. Castelo-Branco, "Cancer stem cells in prostate cancer: implications for targeted therapy," *Urologia internationalis*, vol. 99, no. 2, pp. 125–136, 2017.

[57] A. M. De Marzo, V. L. Marchi, J. I. Epstein, and W. G. Nelson, "Proliferative inflammatory atrophy of the prostate: implications for prostatic carcinogenesis," *The American journal of pathology*, vol. 155, no. 6, pp. 1985–1992, 1999.

[58] M. J. Putzi and A. M. De Marzo, "Morphologic transitions between proliferative inflammatory atrophy and high-grade prostatic intraepithelial neoplasia," *Urology*, vol. 56, no. 5, pp. 828–832, 2000.

[59] I. W. Nelson WG, De Marzo AM, "Prostate cancer," *N Engl J Med*, vol. 3494, pp. 366–381, 2003.

[60] A. M. De Marzo, E. A. Platz, S. Sutcliffe, J. Xu, H. Grönberg, C. G. Drake, Y. Nakai, W. B. Isaacs, and W. G. Nelson, "Inflammation in prostate carcinogenesis," *Nature Reviews Cancer*, vol. 7, no. 4, pp. 256–269, 2007.

[61] A. Thakur, "Nano therapeutic approaches to combat progression of metastatic prostate cancer," *Advances in Cancer Biology-Metastasis*, vol. 2, p. 100009, 2021.

[62] J. A. Halpern, C. Oromendia, J. E. Shoag, S. Mittal, M. F. Cosiano, K. V. Ballman, A. J. Vickers, and J. C. Hu, "Use of digital rectal examination as an adjunct to prostate specific antigen in the detection of clinically significant prostate cancer," *The Journal of urology*, vol. 199, no. 4, pp. 947–953, 2018.

[63] J.-L. Descotes, "Diagnosis of prostate cancer," *Asian journal of urology*, vol. 6, no. 2, pp. 129–136, 2019.

[64] Y. Gong, U. D. Chippada-Venkata, and W. K. Oh, "Roles of matrix metalloproteinases and their natural inhibitors in prostate cancer progression," *Cancers*, vol. 6, no. 3, pp. 1298–1327, 2014.

[65] X. Geng, C. Chen, Y. Huang, and J. Hou, "The prognostic value and potential mechanism of matrix metalloproteinases among prostate cancer," *International Journal of Medical Sciences*, vol. 17, no. 11, p. 1550, 2020.

[66] D. Trudel, Y. Fradet, F. Meyer, and B. Têtu, "Matrix metalloproteinase 9 is associated with gleason score in prostate cancer but not with prognosis," *Human pathology*, vol. 41, no. 12, pp. 1694–1701, 2010.

[67] V. Kasivisvanathan, A. S. Rannikko, M. Borghi, V. Panebianco, L. A. Mynderse, M. H. Vaarala, A. Briganti, L. Budäus, G. Hellawell, R. G. Hindley, *et al.*, "Mri-targeted or standard biopsy for prostate-cancer diagnosis," *New England Journal of Medicine*, vol. 378, no. 19, pp. 1767–1777, 2018.

[68] D. F. Gleason and G. T. Mellinger, "Prediction of prognosis for prostatic adenocarcinoma by combined histological grading and clinical staging," *The Journal of urology*, vol. 111, no. 1, pp. 58–64, 1974.

[69] D. F. Gleason, "Histologic grading of prostate cancer: a perspective," *Human pathology*, vol. 23, no. 3, pp. 273–279, 1992.

[70] U.S. National Institutes of Health, National Cancer Institute, "SEER Training Modules, Prostate cancer." `https://training.seer.cancer.gov/prostate/`, 2023. Accessed May 5, 2023.

[71] P. A. Humphrey, "Gleason grading and prognostic factors in carcinoma of the prostate," *Modern pathology*, vol. 17, no. 3, pp. 292–306, 2004.

[72] J. I. Epstein, W. C. Allsbrook Jr, M. B. Amin, L. L. Egevad, I. G. Committee, *et al.*, "The 2005 international society of urological pathology (isup) consensus conference on gleason grading of prostatic carcinoma," *The American journal of surgical pathology*, vol. 29, no. 9, pp. 1228–1242, 2005.

[73] P. Lawson, A. B. Sholl, J. Q. Brown, B. T. Fasy, and C. Wenk, "Persistent homology for the quantitative evaluation of architectural features in prostate cancer histology," *Scientific reports*, vol. 9, no. 1, p. 1139, 2019.

[74] A. M. Al Nemer, T. Elsharkawy, M. Elshawarby, D. Al-Tamimi, H. Kussaibi, and A. Ahmed, "The updated grading system of prostate carcinoma: an inter-observer agreement study among general pathologists in an academic practice," *Apmis*, vol. 125, no. 11, pp. 957–961, 2017.

[75] J. I. Epstein, L. Egevad, M. B. Amin, B. Delahunt, J. R. Srigley, and P. A. Humphrey, "The 2014 international society of urological pathology (isup) consensus conference on gleason grading of prostatic carcinoma," *The American journal of surgical pathology*, vol. 40, no. 2, pp. 244–252, 2016.

[76] E. I. Verhoef, W. A. van Cappellen, J. A. Slotman, G.-J. Kremers, P. C. Ewing-Graham, A. B. Houtsmuller, M. E. van Royen, and G. J. van Leenders, "Three-dimensional analysis reveals two major architectural subgroups of prostate cancer growth patterns," *Modern Pathology*, vol. 32, no. 7, pp. 1032–1041, 2019.

[77] E. I. Verhoef, W. A. van Cappellen, J. A. Slotman, G.-J. Kremers, P. C. Ewing-Graham, A. B. Houtsmuller, M. E. van Royen, and G. J. van Leenders, "Three-dimensional architecture of common benign and precancerous prostate epithelial lesions," *Histopathology*, vol. 74, no. 7, pp. 1036–1044, 2019.

[78] G. J. van Leenders, E. I. Verhoef, and E. Hollemans, "Prostate cancer growth patterns beyond the gleason score: entering a new era of comprehensive tumour grading," *Histopathology*, vol. 77, no. 6, pp. 850–861, 2020.

[79] J. K. McKenney, W. Wei, S. Hawley, H. Auman, L. F. Newcomb, H. D. Boyer, L. Fazli, J. Simko, A. Hurtado-Coll, D. A. Troyer, *et al.*, "Histologic grading of prostatic adenocarcinoma can be further optimized," *The American journal of surgical pathology*, vol. 40, no. 11, pp. 1439–1456, 2016.

[80] K. A. Iczkowski, K. C. Torkko, G. R. Kotnis, R. Storey Wilson, W. Huang, T. M. Wheeler, A. M. Abeyta, F. G. La Rosa, S. Cook, P. N. Werahera, *et al.*, "Digital quantification of five high-grade prostate cancer patterns, including the cribriform pattern, and their association with adverse outcome," *American journal of clinical pathology*, vol. 136, no. 1, pp. 98–107, 2011.

[81] D. Trudel, M. R. Downes, J. Sykes, K. J. Kron, J. Trachtenberg, and T. H. van der Kwast, "Prognostic impact of intraductal carcinoma and large cribriform carcinoma architecture after prostatectomy in a contemporary cohort," *European Journal of Cancer*, vol. 50, no. 9, pp. 1610–1616, 2014.

[82] C. F. Kweldam, M. F. Wildhagen, E. W. Steyerberg, C. H. Bangma, T. H. Van Der Kwast, and G. J. Van Leenders, "Cribriform growth is highly predictive for postoperative metastasis and disease-specific death in gleason score 7 prostate cancer," *Modern pathology*, vol. 28, no. 3, pp. 457–464, 2015.

[83] J. A. Tuxhorn, G. E. Ayala, and D. R. Rowley, "Reactive stroma in prostate cancer progression," *The Journal of urology*, vol. 166, no. 6, pp. 2472–2483, 2001.

[84] B. M. Baker and C. S. Chen, "Deconstructing the third dimension–how 3d culture microenvironments alter cellular cues," *Journal of cell science*, vol. 125, no. 13, pp. 3015–3024, 2012.

[85] S. M. Dhanasekaran, A. Dash, J. Yu, I. P. Maine, B. Laxman, S. A. Tomlins, C. J. Creighton, A. Menon, M. A. Rubin, and A. M. Chinnaiyan, "Molecular profiling of human prostate tissues: insights into gene expression patterns of prostate development during puberty," *The FASEB Journal 19(2): 1-23*, vol. 19, no. 2, pp. 1–23, 2005.

[86] E. Schaeffer, L. Marchionni, Z. Huang, B. Simons, A. Blackman, W. Yu, G. Parmigiani, and D. Berman, "Androgen-induced programs for prostate epithelial growth and invasion arise in embryogenesis and are reactivated in cancer," *Oncogene*, vol. 27, no. 57, pp. 7180–7191, 2008.

[87] M. Montano and W. Bushman, "Morphoregulatory pathways in prostate ductal development," *Developmental Dynamics*, vol. 246, no. 2, pp. 89–99, 2017.

[88] L. A. Liotta and E. C. Kohn, "The microenvironment of the tumour–host interface," *Nature*, vol. 411, no. 6835, pp. 375–379, 2001.

[89] A. Jabłońska-Trypuć, M. Matejczyk, and S. Rosochacki, "Matrix metalloproteinases (mmps), the main extracellular matrix (ecm) enzymes in collagen degradation, as a target for anticancer drugs," *Journal of enzyme inhibition and medicinal chemistry*, vol. 31, no. sup1, pp. 177–183, 2016.

[90] P. C. Brooks, S. Strömblad, L. C. Sanders, T. L. von Schalscha, R. T. Aimes, W. G. Stetler-Stevenson, J. P. Quigley, and D. A. Cheresh, "Localization of matrix metalloproteinase

mmp-2 to the surface of invasive cells by interaction with integrin $\alpha v\beta 3$," *Cell*, vol. 85, no. 5, pp. 683–693, 1996.

[91] R. Visse and H. Nagase, "Matrix metalloproteinases and tissue inhibitors of metalloproteinases: structure, function, and biochemistry," *Circulation research*, vol. 92, no. 8, pp. 827–839, 2003.

[92] S. Quintero-Fabián, R. Arreola, E. Becerril-Villanueva, J. C. Torres-Romero, V. Arana-Argáez, J. Lara-Riegos, M. A. Ramírez-Camacho, and M. E. Alvarez-Sánchez, "Role of matrix metalloproteinases in angiogenesis and cancer," *Frontiers in oncology*, vol. 9, p. 1370, 2019.

[93] L. M. Coussens, B. Fingleton, and L. M. Matrisian, "Matrix metalloproteinase inhibitors and cancer—trials and tribulations," *Science*, vol. 295, no. 5564, pp. 2387–2392, 2002.

[94] I. Mourkioti, A. Angelopoulou, K. Belogiannis, N. Lagopati, S. Potamianos, E. Kyrodimos, V. Gorgoulis, and A. Papaspyropoulos, "Interplay of developmental hippo–notch signaling pathways with the dna damage response in prostate cancer," *Cells*, vol. 11, no. 15, p. 2449, 2022.

[95] X.-D. Wang, C. C. Leow, J. Zha, Z. Tang, Z. Modrusan, F. Radtke, M. Aguet, F. J. de Sauvage, and W.-Q. Gao, "Notch signaling is required for normal prostatic epithelial cell proliferation and differentiation," *Developmental biology*, vol. 290, no. 1, pp. 66–80, 2006.

[96] P. Carmeliet and R. K. Jain, "Molecular mechanisms and clinical applications of angiogenesis," *Nature*, vol. 473, no. 7347, pp. 298–307, 2011.

[97] B. Belandia, S. M. Powell, J. M. García-Pedrero, M. M. Walker, C. L. Bevan, and M. G. Parker, "Hey1, a mediator of notch signaling, is an androgen receptor corepressor," *Molecular and cellular biology*, vol. 25, no. 4, pp. 1425–1436, 2005.

[98] M. A. Rice, E.-C. Hsu, M. Aslan, A. Ghoochani, A. Su, and T. Stoyanova, "Loss of notch1 activity inhibits prostate cancer growth and metastasis and sensitizes prostate cancer cells to antiandrogen therapiesloss of notch1 as a therapeutic strategy for prostate cancer," *Molecular cancer therapeutics*, vol. 18, no. 7, pp. 1230–1242, 2019.

[99] J. Shou, S. Ross, H. Koeppen, F. J. de Sauvage, and W.-Q. Gao, "Dynamics of notch expression during murine prostate development and tumorigenesis," *Cancer research*, vol. 61, no. 19, pp. 7291–7297, 2001.

[100] B. Bin Hafeez, V. M. Adhami, M. Asim, I. A. Siddiqui, K. M. Bhat, W. Zhong, M. Saleem, M. Din, V. Setaluri, and H. Mukhtar, "Targeted knockdown of notch1 inhibits invasion of human prostate cancer cells concomitant with inhibition of matrix metalloproteinase-9 and urokinase plasminogen activator," *Clinical cancer research*, vol. 15, no. 2, pp. 452–459, 2009.

[101] Y. Zhang, Z. Wang, F. Ahmed, S. Banerjee, Y. Li, and F. H. Sarkar, "Retracted: Down-regulation of jagged-1 induces cell growth inhibition and s phase arrest in prostate cancer cells," *International journal of cancer*, vol. 119, no. 9, pp. 2071–2077, 2006.

[102] F. L. Carvalho, B. W. Simons, C. G. Eberhart, and D. M. Berman, "Notch signaling in prostate cancer: a moving target," *The Prostate*, vol. 74, no. 9, pp. 933–945, 2014.

[103] Y. Qing, Y. Wang, C. Hu, H. Zhang, Z. Zhang, T. Ma, S. Zhang, K. Li, *et al.*, "Evaluation of notch family genes' expression and prognostic value in prostate cancer," *Translational Andrology and Urology*, vol. 11, no. 5, p. 627, 2022.

[104] L.-Q. Chen, "Phase-field models for microstructure evolution," *Annual review of materials research*, vol. 32, no. 1, pp. 113–140, 2002.

[105] A. A. Wheeler, W. J. Boettinger, and G. B. McFadden, "Phase-field model for isothermal phase transitions in binary alloys," *Physical Review A*, vol. 45, no. 10, p. 7424, 1992.

[106] J. Löber, F. Ziebert, and I. S. Aranson, "Modeling crawling cell movement on soft engineered substrates," *Soft matter*, vol. 10, no. 9, pp. 1365–1373, 2014.

[107] R. Kobayashi, "Modeling and numerical simulations of dendritic crystal growth," *Physica D: Nonlinear Phenomena*, vol. 63, no. 3-4, pp. 410–423, 1993.

[108] R. D. Travasso, M. Castro, and J. C. Oliveira, "The phase-field model in tumor growth," *Philosophical Magazine*, vol. 91, no. 1, pp. 183–206, 2011.

[109] R. Qin and H. Bhadeshia, "Phase field method," *Materials science and technology*, vol. 26, no. 7, pp. 803–811, 2010.

[110] D. Tourret, H. Liu, and J. LLorca, "Phase-field modeling of microstructure evolution: Recent applications, perspectives and challenges," *Progress in Materials Science*, vol. 123, p. 100810, 2022.

[111] M. Fritz, "Tumor evolution models of phase-field type with nonlocal effects and angiogenesis," *Bulletin of Mathematical Biology*, vol. 85, no. 6, p. 44, 2023.

[112] S. M. Allen and J. W. Cahn, "A microscopic theory for antiphase boundary motion and its application to antiphase domain coarsening," *Acta metallurgica*, vol. 27, no. 6, pp. 1085–1095, 1979.

[113] F. Tadayyon, M. Mellat, F. Alizadeh, M. Hadi, M. Khorrami, M. Yazdani, and R. H. Joozdani, "Prostate cancer: Relationship between vascular diameter, shape and density and gleason score in needle biopsy specimens," *Advanced Biomedical Research*, vol. 2, 2013.

[114] A. S. D. Morais, *Development of a Prostate Cancer Computational Model*. PhD thesis, Universidade de Coimbra, 2021.

[115] F. Paiva, "Influence of the underlining duct structure in prostate adenocarcinoma progression," 2022.

[116] T. Biben, K. Kassner, and C. Misbah, "Phase-field approach to three-dimensional vesicle dynamics," *Physical Review E*, vol. 72, no. 4, p. 041921, 2005.

[117] R. D. Travasso, O. Kuksenok, and A. C. Balazs, "Exploiting photoinduced reactions in polymer blends to create hierarchically ordered, defect-free materials," *Langmuir*, vol. 22, no. 6, pp. 2620–2628, 2006.

[118] R. D. Travasso, O. Kuksenok, and A. C. Balazs, "Harnessing light to create defect-free, hierarchically structured polymeric materials," *Langmuir*, vol. 21, no. 24, pp. 10912–10915, 2005.

[119] G. Lorenzo, "Tissue-scale, patient-specific modeling and simulation of prostate cancer growth," 2018.